Asari, S., Lesur, V. (2011): Radial vorticity constraint in core flow modeling. - Journal of Geophysical Research, 116, B11101

DOI: 10.1029/2011JB008267

Radial vorticity constraint in core flow modeling

S. Asari[1] and V. Lesur[1]

Received 2 February 2011; revised 8 August 2011; accepted 9 August 2011; published 9 November 2011.

[1] We present a new method for estimating core surface flows by relaxing the tangentially geostrophic (TG) constraint. Ageostrophic flows are allowed if they are consistent with the radial component of the vorticity equation under assumptions of the magnetostrophic force balance and an insulating mantle. We thus derive a tangentially magnetostrophic (TM) constraint for flows in the spherical harmonic domain and implement it in a least squares inversion of *GRIMM-2*, a recently proposed core field model, for temporally continuous core flow models (2000.0–2010.0). Comparing the flows calculated using the TG and TM constraints, we show that the number of degrees of freedom for the poloidal flows is notably increased by admitting ageostrophic flows compatible with the TM constraint. We find a significantly improved fit to the *GRIMM-2* secular variation (SV) by including zonal poloidal flow in TM flow models. Correlations between the predicted and observed length-of-day variations are equally good under the TG and TM constraints. In addition, we estimate flow models by imposing the TM constraint together with other dynamical constraints: either purely toroidal (PT) flow or helical flow constraint. For the PT case we cannot find any flow which explains the observed SV, while for the helical case the SV can be fitted. The poor compatibility between the TM and PT constraints seems to arise from the absence of zonal poloidal flows. The PT flow assumption is likely to be negated when the radial magnetostrophic vorticity balance is taken into account, even if otherwise consistent with magnetic observations.

Citation: Asari, S., and V. Lesur (2011), Radial vorticity constraint in core flow modeling, *J. Geophys. Res.*, *116*, B11101, doi:10.1029/2011JB008267.

1. Introduction

[2] Horizontal flows of the electrically conducting fluid at the Earth's core surface advect the magnetic field, resulting in temporal variations of the observed global geomagnetic field. Satellite magnetic field monitoring over the last decade has revealed the spatial and temporal structures of the core main field (MF) with increasing accuracy, probably up to its smallest-scale components that are unaffected by the noise from other sources. Core surface flow modeling has come to a phase, in which even temporal fluctuations of the flow are discussed in association with subdecadal changes of magnetic field and Earth rotation [*Holme and Olsen*, 2006; *Wardinski et al.*, 2008]. It has been reported that such rapid changes of the flow are actually required to explain the recent fluctuations of secular variation (SV) [*Olsen and Mandea*, 2008]. Meanwhile, there still remain obstacles in better resolving the core surface flow. A significant error in flow imaging arises from the unmodeled SV due to the advection of the small-scale MF masked by the crustal field [*Eymin and Hulot*, 2005]. Instead of fitting the observed SV tightly, one needs to allow for a possible error from the unmodeled SV [*Pais and Jault*, 2008; *Gillet et al.*, 2009]. The theoretical non-uniqueness problem in the flow modeling [e.g., *Holme*, 2007] is another setback which is even more serious. Assumptions used to alleviate the flow uncertainty can distort resulting flow images more significantly than the errors estimated for the unmodeled SV. Choices of assumptions are thus a critical matter in flow modeling.

[3] Various assumptions have been proposed and implemented in core surface flow modeling. These are typically based on dynamics relevant to core flow, such as tangentially geostrophic (TG) flow, purely toroidal (PT) flow and helical flow [see, e.g., *Holme*, 2007], as well as the recent quasi-geostrophic flow [*Pais and Jault*, 2008]. Among these the TG assumption has been most commonly employed, in which the Lorentz force is eliminated from the horizontal force balance at the core surface, resulting in TG equilibrium. It has been adopted not only to model the core flow but also to compute the fluid pressure [*Chulliat and Hulot*, 2000; *Chambodut et al.*, 2007] and the accompanying pressure torque acting on the topography of the mantle's bottom [e.g., *Jault and Le Mouël*, 1989; *Greff-Lefftz and Legros*, 1995]. However, the TG assumption is known to have theoretical and observational difficulties. First of all, it necessarily fails at the geographical equator, where the horizontal Coriolis force vanishes. The TG constraint alters the configuration of estimated flows significantly at the geographic equator, restricting flows to only the azimuthal component. As a result,

[1]Helmholtz-Zentrum Potsdam, Deutsches GeoForschungsZentrum, Potsdam, Germany.

0148-0227/11/2011JB008267

estimated TG flow models tend to fail in explaining the local SV around the equator [*Wardinski et al.*, 2008]. Furthermore, recent analyses have found that a pure TG flow model has difficulty in explaining the time variation of satellite SV models [*Olsen and Mandea*, 2008; *Wardinski et al.*, 2008].

[4] Recently, *Gillet et al.* [2010] proposed a model of fast torsional waves in the fluid core, by analyzing the nearly six-year periodicity of the length-of-day (LOD) observation. In their model, the magnetic field inside the core has intensities of several mT (an order of magnitude greater than the radial field at the core surface), causing torsional waves in correlation with the rapid LOD variation. It is then implied that the core is in a state with the toroidal field dominating the poloidal field, rather than with their magnitudes being comparable [*Busse*, 1975]. Meanwhile, the TG assumption has been essentially based on weaker field within the core (the intensity of several tenths of mT [e.g., *Busse*, 1975]) in neglecting the Lorentz force [*Le Mouël et al.*, 1985; *Jault and Le Mouël*, 1991a]. The strong magnetic field, associated with the strong electric current, may amount to the Lorentz force playing an important role even near the core-mantle boundary (CMB). All the above arguments suggest that the TG constraint be relaxed to some extent, so that subsequent flow models may be consistent with both theory and observations. Flow models estimated with relaxed TG constraints have already been investigated [*Pais et al.*, 2004], where the constraint is imposed in a weak form associated with a damping parameter controlling the degree of the relaxation. This numerically motivated approach has nonetheless shown that the TG constraint starts to relax particularly from the vicinity of the geographic equator.

[5] In this paper we develop a more physically motivated method to relax the TG constraint, letting the flow respect the radial component of vorticity equation in magnetostrophic balance at the core surface. This equation (simply referred to as radial vorticity (RV) equation in this paper) has already been discussed in the context of MF modeling. Under the assumptions of a perfectly electrically conducting core and an insulating mantle, the RV equation yields a useful constraint on the time evolution of the radial magnetic field at the CMB (RV constraint) [*Gubbins*, 1991; *Jackson*, 1996]. It has been demonstrated that magnetic observations for the past hundred years do not contradict the RV constraint [*Jackson et al.*, 2007], which implies that the pure TG flow assumption is valid. It should be noted that ageostrophic (i.e., non-TG) flow is also allowed to exist, because the TG constraint is only a sufficient condition of the RV constraint (section 2). Here, we build a flow model with purely TG flow (which necessarily satisfies the RV constraint) supplemented by ageostrophic flow, yet restricting the latter to the elements compatible with the RV equation.

[6] The RV equation can be used to constrain a core flow model in combination with other flow constraints, such as a purely toroidal (PT) flow constraint. Indeed, the PT flow assumption is motivated by a magnetostrophic balance near the core surface, involving only toroidal flows consisting conceivably of (purely zonal) geostrophic flows and horizontally polarized slow MAC-waves [*Bloxham*, 1990]. Likewise, a helical flow model may well satisfy the RV equation. With reference to the fit to magnetic observations alone, previous works have investigated both the assumptions of PT flow [*Holme and Olsen*, 2006; *Wardinski et al.*, 2008] and helical flow [*Amit and Olson*, 2004]. Here, we seek for the presence of reasonable flow models compatible with the RV equation and either of these assumptions. This would provide an observational insight as to the consistency of these two flow assumptions with the magnetostrophic balance.

[7] We begin in section 2 with a review of the RV equation and introduce the tangentially magnetostrophic (TM) constraint for the core flow. Our method of flow modeling is described in section 3, while the practical part of implementing the TM constraint is given in detail in Appendix A. The results of flow modeling with the RV constraint are presented in section 4. The results obtained by including additional PT or helical flow constraints then follow in section 5. Sections 6 and 7 are discussion and conclusions, respectively.

2. Radial Vorticity Equation and Tangentially Magnetostrophic Constraint

[8] We here follow the derivation of the RV equation in the same framework as *Gubbins* [1991]. His analysis focuses on temporal and spatial scales relevant to the observational studies of the SV and core flow. The fluid core dynamics are described by the "slow-steady equations," where the inertial terms are eliminated from relevant equations. Neglecting the viscous term in the Navier-Stokes equation in the Boussinesq approximation, the magnetostrophic balance reads

$$2\rho\boldsymbol{\Omega}\times\boldsymbol{u} = -\nabla p + A\hat{\boldsymbol{r}} + \boldsymbol{J}\times\boldsymbol{B}, \tag{1}$$

where ρ is the core fluid density, $\boldsymbol{\Omega}$ the angular velocity of the Earth rotation, $\boldsymbol{u}$ the core flow, p the dynamical pressure, $A\hat{\boldsymbol{r}}$ the radial buoyancy with $\hat{\boldsymbol{r}}$ being the radial unit vector, $\boldsymbol{J}$ the electric current density and $\boldsymbol{B}$ the magnetic field.

[9] The buoyancy term can be excluded by operating on equation (1) with $-\hat{\boldsymbol{r}}\times$:

$$\rho f \boldsymbol{u}_H = -\nabla\times p\hat{\boldsymbol{r}} + \left(J_r\boldsymbol{B}_H - B_r\boldsymbol{J}_H\right), \tag{2}$$

where $f \equiv 2\Omega\cos\theta$ is the radial component of the planetary vorticity. Here spherical coordinates are useful, with (r, θ, φ) denoting radial, meridional and azimuthal components, respectively; the subscript H denotes the horizontal components. Note that the radial flow u_r near the core surface is neglected in deriving equation (2), considering the solid boundary right above. One can further let $J_r = 0$ in equation (2) for an electrically insulating mantle, which has been commonly considered as a reasonable approximation in dealing with the MF at the time and spatial scales of interest (this shall be discussed later in section 6). Now the equation becomes tractable, as the horizontal magnetic field $\boldsymbol{B}_H$ comprising the (observationally unknown) toroidal component has been eliminated. The Lorentz contribution remaining in equation (2) arises only from the radial MF B_r and the horizontal electric current $\boldsymbol{J}_H$. The assumption of insulating mantle allows us to map the large-scale B_r at and near the core surface by the downward continuation of magnetic observations.

[10] The RV equation is concerned with the solenoidal part of horizontal force balance, or magnetostrophic balance

Table 1. Values and Typical Scales of Physical Quantities

Description	Notation	Value
Earth radius	a	6371.2 km
Core radius	c	3485.0 km
Core density	ρ	1.2×10^4 kg/m^3
Earth angular velocity	Ω	7.3×10^{-5} rad/s
Magnetic permeability	μ_o	$4\pi \times 10^{-7}$ H/m
Core electric conductivity	σ_c	5×10^5 S/m
Radial field at CMB	$\mathcal{P}$	5×10^{-4} T
Flow velocity	$\mathcal{V}$	5×10^{-4} m/s
Field and flow length scale	$\mathcal{L}$	10^3 km
SV time constant	τ	10 years
Mantle conductivity	σ_m	10^3 S/m
Mantle conducting layer thickness	Δ_m	10^2 km

here. Near the core surface it is given by the horizontal divergence of equation (2):

$$G(\boldsymbol{u}_H(\theta,\varphi)) = -\nabla_H \cdot (B_r \boldsymbol{J}_H)\,, \tag{3}$$

where G denotes the radial planetary vorticity advection:

$$G(\boldsymbol{u}_H(\theta,\varphi)) \equiv \rho \nabla_H \cdot (f\,\boldsymbol{u}_H)\,. \tag{4}$$

The RV equation (3) can be compared, in a mathematical analogy, to the radial induction equation (7) [*Gubbins*, 1991]; the RV advection G and horizontal electric current $\boldsymbol{J}_H$ are replaced with the radial SV $\dot{B}_r$ and core surface flow $\boldsymbol{u}_H$, respectively.

[11] The RV equation (3) leads to a set of constraints on the time evolution of the MF. Surface integration of the RV equation with respect to a so-called null-flux patch C (a fragment of the spherical CMB delineated by the null-flux curve ∂C given as a closed contour of $B_r = 0$) yields

$$\int_C G\, dS = 0 \tag{5}$$

and consequently [*Jackson*, 1996; *Chulliat and Hulot*, 2001]

$$\frac{d}{dt}\int_C f\, dS = 0\,. \tag{6}$$

It states that the MF has to evolve in time such that every C migrates or deforms the way the flux of radial planetary vorticity f is conserved. The constraint (6) has been referred to as the "RV constraint" and used to constrain MF models [*Jackson et al.*, 2007].

[12] In this work we use the RV equation (3) to add a constraint on the core flow $\boldsymbol{u}_H$. Our flow modeling relies basically on the radial component of the induction equation near the core surface [*Bloxham and Jackson*, 1991]:

$$\dot{B}_r = -\nabla_H \cdot (B_r \boldsymbol{u}_H) \tag{7}$$

(the overdot indicates a derivative with respect to time t). In equation (7) the diffusion term has already been neglected on the basis of the frozen-flux assumption [*Roberts and Scott*, 1965]. It then follows that $\boldsymbol{J}_H$ in the RV equation (3) is purely poloidal, since the diffusion term in the radial induction equation relates directly to the toroidal part of $\boldsymbol{J}_H$ [*Pais et al.*, 2004]. Our new constraint for the flow to meet this RV equation will be referred to as "tangentially magnetostrophic (TM) constraint," its subsequent model having a form of "TM flow":

$$\begin{aligned} \boldsymbol{u}_H^{TM} &= -\frac{1}{\rho f}(\nabla \times p\hat{\boldsymbol{r}} + B_r \boldsymbol{J}_H) \\ &= -\frac{1}{\rho f}\left(\nabla \times (p+p_m)\hat{\boldsymbol{r}} + (B_r \boldsymbol{J}_H)_P\right). \end{aligned} \tag{8}$$

The second expression of $\boldsymbol{u}_H^{TM}$ in equation (8) is derived by splitting $B_r \boldsymbol{J}_H$ into its poloidal part $(B_r \boldsymbol{J}_H)_P$ and toroidal part $(B_r \boldsymbol{J}_H)_T$ ($= \nabla \times p_m \hat{\boldsymbol{r}}$, with p_m being the magnetic pressure). The constituent $\boldsymbol{u}_H^{TG} = -(\rho f)^{-1}\nabla \times (p+p_m)\hat{\boldsymbol{r}}$ of the TM flow $\boldsymbol{u}_H^{TM}$ may be named TG flow, as it satisfies the TG constraint [*Le Mouël et al.*, 1985]:

$$G(\boldsymbol{u}_H(\theta,\varphi)) = 0\,, \quad \forall\,(\theta,\varphi)\,. \tag{9}$$

The TG constraint is a particular case of the RV equation (3) when $\boldsymbol{J}_H$ is such that $(B_r \boldsymbol{J}_H)_P = 0$, so a pure TG flow $\boldsymbol{u}_H^{TG}$ is regarded to meet the TM constraint as well.

[13] To further discuss the TM constraint, let us consider a complete flow space U, the linear space of tangential vector fields over the spherical surface with the mean core radius c (Table 1). A physically meaningful inner product relevant to U may be

$$\langle \boldsymbol{u}_H^1, \boldsymbol{u}_H^2 \rangle_c = \frac{1}{4\pi c^2}\oint_{r=c} \boldsymbol{u}_H^1 \cdot \boldsymbol{u}_H^2\, dS\,, \tag{10}$$

where the integral is taken with respect to the whole core surface (the associated square norm $\|\boldsymbol{u}_H\|_c^2$ ($= \langle \boldsymbol{u}_H, \boldsymbol{u}_H \rangle_c$) represents the total kinetic energy of $\boldsymbol{u}_H$ over the spherical surface). We note that TM flows $\boldsymbol{u}_H^{TM}$ form a linear subspace U_{TM} of U; the TM flow space U_{TM} includes only TM flow elements that are compatible with the RV equation (3) for each associated pressure ($p + p_m$) and poloidal electric current $\boldsymbol{J}_H$ (note that B_r is already given). Furthermore, TG flows $\boldsymbol{u}_H^{TG}$ satisfying the TG constraint (9) form a linear subspace U_{TG} of U_{TM}. We thus have $U_{TG} \subset U_{TM} \subset U$. The TM constraint is therefore a relaxed one relative to the TG constraint; the former restricts the model flow space to U_{TM}, while the latter restricts the model flow space to U_{TG}.

[14] An arbitrary flow $\boldsymbol{u}_H^o$ given in U can be sorted as

$$\boldsymbol{u}_H^o = \boldsymbol{u}_H^{TG} + \boldsymbol{u}_H^{ATM} + \boldsymbol{u}_H^{NM}\,. \tag{11}$$

The first constituent is a pure TG flow $\boldsymbol{u}_H^{TG} \in U_{TG}$; the second is an "ageostrophic TM" flow $\boldsymbol{u}_H^{ATM} \in U_{TM}$ yet $\notin U_{TG}$, e.g., a flow causing a RV advection G_{ATM} consistent with the RV constraint (5) but inconsistent with the TG constraint (9); the last is a "non-magnetostrophic" flow $\boldsymbol{u}_H^{NM} \notin U_{TM}$, e.g., a flow causing a RV advection G_{NM} inconsistent with the RV constraint (5). The flow classification (11) can be reorganized as

$$\boldsymbol{u}_H^o = \boldsymbol{u}_H^{TM} + \boldsymbol{u}_H^{NM} \tag{12}$$

or

$$\boldsymbol{u}_H^o = \boldsymbol{u}_H^{TG} + \boldsymbol{u}_H^{AG}, \tag{13}$$

where $\boldsymbol{u}_H^{TM} = \boldsymbol{u}_H^{TG} + \boldsymbol{u}_H^{ATM}$ forms the TM flow part and

$$\boldsymbol{u}_H^{AG} = \boldsymbol{u}_H^{ATM} + \boldsymbol{u}_H^{NM} \tag{14}$$

forms the ageostrophic flow part.

[15] It is possible to perform the flow separation (11) so that all the three flow parts may become orthogonal to one another with respect to the inner product (10). This orthogonal decomposition means a simple relation for flow kinetic energy $\|\boldsymbol{u}_H^o\|_c^2 = \|\boldsymbol{u}_H^{TG}\|_c^2 + \|\boldsymbol{u}_H^{ATM}\|_c^2 + \|\boldsymbol{u}_H^{NM}\|_c^2$. Further, we specify the three parts such that $\|\boldsymbol{u}_H^{TG}\|_c^2$ is maximized and $\|\boldsymbol{u}_H^{NM}\|_c^2$ is minimized among all possible choices for each. Indeed, the decomposition (13) has been made in the same manner in previous studies [e.g., *Bloxham*, 1989; *Wardinski et al.*, 2008].

[16] We develop projection operators P_{TG}, P_{ATM} and P_{NM} based on the inner product (10) so that we can derive each flow part as

$$\boldsymbol{u}_H^{TG} = P_{TG}\boldsymbol{u}_H^o, \boldsymbol{u}_H^{ATM} = P_{ATM}\boldsymbol{u}_H^o \text{ and } \boldsymbol{u}_H^{NM} = P_{NM}\boldsymbol{u}_H^o.$$

[17] In the flow modeling with the TG constraint, the kinetic energy of ageostrophic flow $\|\boldsymbol{u}_H^{AG}\|_c^2$ is damped completely, i.e., $\boldsymbol{u}_H^{ATM}$ and $\boldsymbol{u}_H^{NM}$ are to be excluded altogether from a TG flow model. With the TM constraint, the TM flow part is left unconstrained and the kinetic energy of non-magnetostrophic flow $\|\boldsymbol{u}_H^{NM}\|_c^2$ is alone damped completely.

3. Core Flow Inversion With the TM Constraint in the Spherical Harmonic Domain

[18] In order to apply the TM constraint to the core flow modeling, we consider a practical method in which all the computations are to be performed in the spherical harmonic (SH) domain. We expand the RV equation (3) and FF induction equation (7) in the Schmidt's quasi-normalized SH function $Y_l^m(\theta, \varphi)$ (hereafter l always denotes the SH degree). The latter turns out to be

$$\dot{\mathsf{b}} = \mathsf{A}_{\dot{\mathsf{b}}}\mathsf{m}, \tag{15}$$

where the column vector $\dot{\mathsf{b}}$ contains the SV Gauss coefficients, m the SH coefficients of the toroidal and poloidal scalar functions of the core surface flow $\boldsymbol{u}_H$, and $\mathsf{A}_{\dot{\mathsf{b}}}$ is the matrix whose elements are linear functions of the MF Gauss coefficients [*Whaler*, 1986]. It is worth remarking that, by virtue of the identity of equations (3) and (7) in terms of their analytical forms, the RV equation can be expressed in the SH domain as

$$\mathsf{g} = \mathsf{A}_{\mathsf{g}}\mathsf{j}, \tag{16}$$

with the matrix A_{g} being the same as $\mathsf{A}_{\dot{\mathsf{b}}}$ if $\dot{B}_r$ is defined with respect to the CMB. The column vector g contains the SH coefficient of the radial planetary vorticity advection G. j represents coefficients of the electric current $\boldsymbol{J}_H$, but here we restrict it to the poloidal component alone (and A_{g} to its relevant part), because the toroidal electric current has already been ruled out under the frozen-flux assumption as in equation (7) [*Pais et al.*, 2004].

[19] The MF and SV coefficients are supplied by our latest geomagnetic field model *GRIMM-2* for 2000.0–2010.0 [*Lesur et al.*, 2010b]. *GRIMM-2* is a model built using data from the satellite CHAMP and ground-based observatories. It consists of Gauss coefficients expanded in time in the B-spline function of order 6 with knot spacings of 1.0 year. We use its internal field components up to SH degree $L_B = 14$ for the SV coefficients to form $\dot{\mathsf{b}}$ and for the MF coefficients to calculate $\mathsf{A}_{\dot{\mathsf{b}}}$ and A_{g}. The toroidal and poloidal flows are truncated at SH degree $L_u = 27$ (i.e., $\boldsymbol{u}_H$ is parameterized by $2L_u(L_u + 2) = 1566$ coefficients for a given epoch). This flow yields the vorticity advection g up to degree $L_G = L_u + 1 = 28$, so we should consider the TM constraint up to degree 28. Further, we take $L_J = 14$ for the truncation degree of the horizontal poloidal electric current j, so that it may lead to the Lorentz vorticity forcing $\mathsf{A}_{\mathsf{g}}\mathsf{j}$ up to degree $L_J + L_B = 28$ ($= L_G$), when the MF is truncated at degree $L_B = 14$. All the coefficients m, g and j are expanded in time based on the same B-spline function as employed in *GRIMM-2*.

[20] Flow models are inferred by means of the penalized least squares method. We minimize an objective function,

$$\Phi = \frac{1}{t_1 - t_0}\int_{t_0}^{t_1} \Phi_t \, dt, \tag{17}$$

where $t_0 = 2000.0$ and $t_1 = 2010.0$ denote the starting and ending years of modeling period, respectively, and

$$\Phi_t(\mathsf{m}) = \left(\dot{\mathsf{b}} - \mathsf{A}_{\dot{\mathsf{b}}}\mathsf{m}\right)^T \mathsf{C}_{\dot{\mathsf{b}}}^{-1}\left(\dot{\mathsf{b}} - \mathsf{A}_{\dot{\mathsf{b}}}\mathsf{m}\right) + Q(\mathsf{m}) + R(\mathsf{m}) + S(\mathsf{m}). \tag{18}$$

$\mathsf{C}_{\dot{\mathsf{b}}}$ and S are a SV covariance matrix and a regularization norm for temporal and spatial smoothness, respectively. These are specified later in this section. Q and R are related to the physical constraints:

[21] 1. Q ($\equiv \lambda_q \mathsf{m}^T \mathsf{D}_q^{-1}\mathsf{m}$) is a semi-norm for the TG constraint or TM constraint, where λ_q is the damping parameter and D_q^{-1} is the damping matrix representing either of D_{TG}^{-1} for the TG constraint (whereby $\boldsymbol{u}_H^{AG}$ is damped) or D_{TM}^{-1} for the TM constraint (whereby only $\boldsymbol{u}_H^{NM}$ is damped). In Appendix A, these matrices are derived by analyzing the matrix A_{g}.

[22] 2. R ($\equiv \lambda_r \mathsf{m}^T \mathsf{D}_r^{-1}\mathsf{m}$) is a (semi-)norm for the additional physical or geometric constraints. We here particularly consider the assumptions of PT and helical flows, deriving D_r^{-1} for them in Appendix B. We just note here that, in the strict helical flow assumption, the degree of freedom of the flow model space is reduced by half (just as in the PT flow assumption) due to a proportionality between the flow upwelling $\xi \equiv \nabla_h \cdot \boldsymbol{u}_H$ and radial component of *relative* vorticity $\zeta \equiv \hat{\boldsymbol{r}} \cdot \nabla \times \boldsymbol{u}_H$ near the core surface [*Amit and Olson*, 2004].

[23] The temporal integration of Φ_t given in equation (17) is performed by means of the Gauss-Legendre quadrature. We exactly integrate the polynomial of degree 12 by taking 11 samplings t_i per each 1-year knot interval of B-splines ($i = 1, \cdots, 110$ for the whole modeling period).

[24] In the previous core flow inversions based on satellite magnetic models, the SV covariance matrix $\mathsf{C}_{\dot{\mathsf{b}}}$ has been quantified by considering different sources of SV variance:

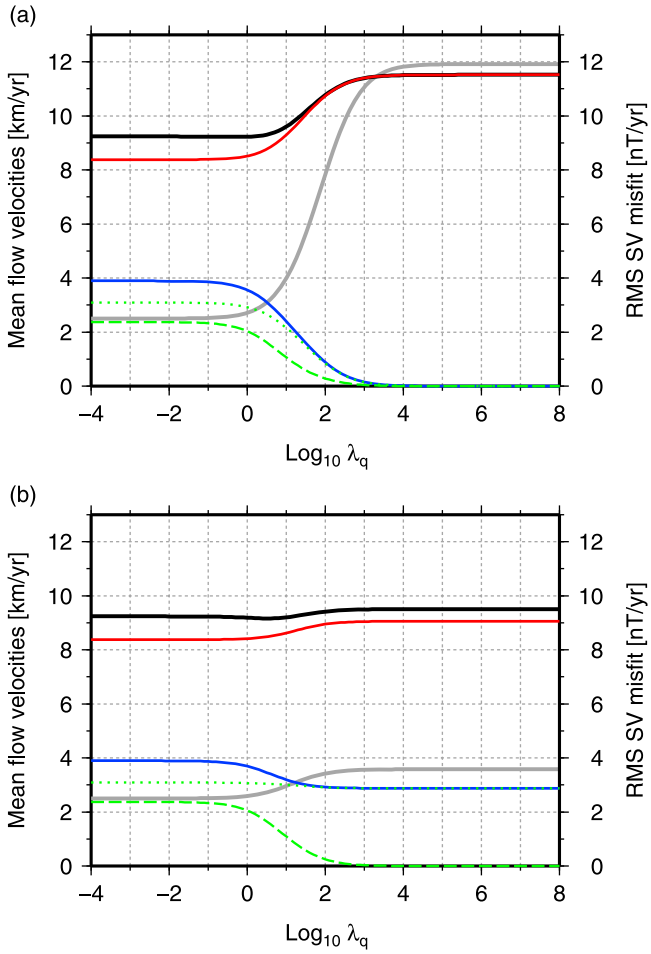

Figure 1. The mean flow velocities (in km/yr) at 2005.0 as a function of the damping parameter λ_q. For the (a) TG constraint and (b) TM constraint, the mean velocities of the total flows $\|\boldsymbol{u}_H\|_c$ (black), its TG components $\|\boldsymbol{u}_H^{TG}\|_c$ (red), ageostrophic components $\|\boldsymbol{u}_H^{AG}\|_c$ (blue), ageostrophic TM components $\|\boldsymbol{u}_H^{ATM}\|_c$ (dotted green) and non-magnetostrophic components $\|\boldsymbol{u}_H^{NM}\|_c$ (dashed green) are plotted. Also shown are the RMS SV misfits $(\|\delta\dot{\boldsymbol{B}}\|_a^2)^{\frac{1}{2}}$ (in nT/yr) at the Earth's surface for the whole model period 2000.0–2010.0 (gray).

[25] 1. Satellite SV models such as *GRIMM-2* are still subject to "observation and modeling error," while the amount, coverage and accuracy of magnetic data have been substantially enhanced. A rough (but not too optimistic) estimate of SV variance for *GRIMM-2* would be 0.5 nT^2/yr^2 per SH degree evenly at the Earth's surface.

[26] 2. SV due to magnetic diffusion at the CMB has been crudely estimated by calculating the "free decay" of the field assuming the absence of core flow [*Holme and Olsen*, 2006]. In particular, the free decay of the axial dipole mode can be the most important ingredient of diffusion to be allowed for as SV misfit.

[27] 3. The large-scale SV may also be attributed to "non-modeled advection," i.e., advection of the small-scale MF truncated and neglected in the flow modeling [*Eymin and Hulot*, 2005]. Hence, a flow model estimated without accounting for this SV contribution can be affected by the aliasing. The SV misfit may even have to be no smaller than those of flow models based on magnetic models built with ground-based observation alone [*Pais and Jault*, 2008].

[28] In this study, we set the SV covariance matrix in the objective function (18) using the observation error and the field free decay, following the manner of *Holme and Olsen* [2006]. More specifically, we let

$$\mathsf{C}_{\dot{\mathsf{b}}} = \mathrm{diag}\left[\frac{0.5}{(l+1)(2l+1)} + \left(\dot{g}_{l,m}^{D}\right)^2\right]. \tag{19}$$

Here, we use the free decay SV $\dot{g}_{l,m}^{D} = -(k_l^n)^2(\eta_c/c^2)g_l^m$, where $\eta_c = (\mu_o\sigma_c)^{-1}$ is the magnetic diffusivity, with the magnetic permeability μ_o and the electric conductivity of the core σ_c (Table 1). k_l^n denotes the nth zero of the degree $l-1$ spherical Bessel function, and in this particular calculation we let $n = l$. Recent studies have estimated flow models fitting SV models either at one standard deviation [*Pais and Jault*, 2008] or even more tightly [*Holme and Olsen*, 2006; *Olsen and Mandea*, 2008; *Wardinski et al.*, 2008]. Here, we do not restrict ourselves to either of these cases, but study resulting models by varying the misfit level within one standard deviation. The effect of aliasing due to the small-scale MF truncation is evaluated for each flow model a posteriori. The regularization norm S for the model smoothness (18) is given by

$$S(\mathsf{m}) = \lambda_s \mathsf{m}^T\mathsf{D}_s^{-1}\mathsf{m} + \lambda_t \mathsf{m}^T\mathsf{D}_t^{-1}\mathsf{m}. \tag{20}$$

The first term denotes the norm for the spatial smoothness, for which we adapt the norm $\mathsf{D}_s^{-1} = \mathrm{diag}[l^2(l+1)^2/(2l+1)]$ [*Gillet et al.*, 2009; *Lesur et al.*, 2010a]. We do not choose the "strong norm" [*Bloxham*, 1988] which has been most commonly used [*Holme and Olsen*, 2006; *Wardinski et al.*, 2008], because it may overdamp the small-scale flows. The second term is for the temporal smoothness; D_t^{-1} is a positive definite matrix such that $\mathsf{m}^T\mathsf{D}_t^{-1}\mathsf{m} = \|\partial_t \boldsymbol{u}_H\|_c^2$. We add the temporal smoothness simply for the purpose of regularization, so λ_t is fixed at 1.0×10^{-6} in this study.

4. Core Flow Models Estimated With TM Constraint

[29] In this section, we present flow models estimated with the TM and TG constraints and compare their properties. We consider the PT or helical flow constraint in the next section, so the damping parameter λ_r is set to be 0 for now. To see how the TM constraint regulates the flow solution, we first derive two flow models using the semi-norm Q (in equation (18)) with its damping matrix D_q^{-1} tuned for the TG and TM constraints. In this particular analysis, we fix the damping parameters λ_s at 1.0×10^{-1}. From the resulting flow models $\boldsymbol{u}_H$ with a wide range of the damping parameter λ_q, we compute the RMS velocity $\|\boldsymbol{u}_H\|_c$ at 2005.0, as well as its TG part $\|\boldsymbol{u}_H^{TG}\|_c$, ageostrophic TM part $\|\boldsymbol{u}_H^{ATM}\|_c$ and non-magnetostrophic part $\|\boldsymbol{u}_H^{NM}\|_c$ (Figure 1). Obviously, the TM constraint damps only $\boldsymbol{u}_H^{NM}$, whereas the TG constraint damps both $\boldsymbol{u}_H^{ATM}$ and $\boldsymbol{u}_H^{NM}$. It is remarkable that these two constraints damp $\boldsymbol{u}_H^{NM}$ with nearly the same efficiency (the green dashed curves in Figures 1a and 1b behave almost in the same manner). The magnitude of

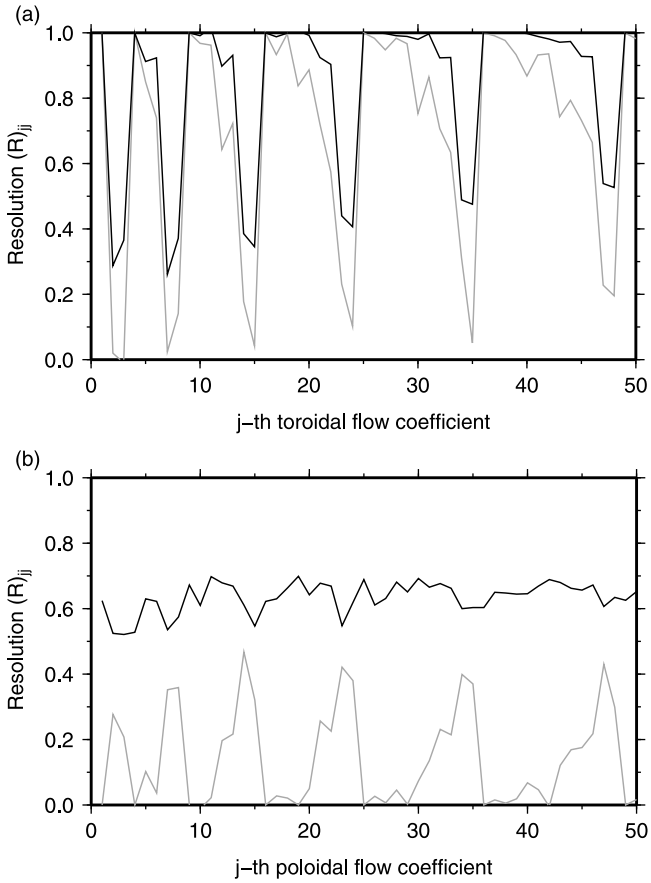

Figure 2. The diagonal elements of the resolution matrix R defined by equation (21), computed with the regularization matrix D_q^{-1} for the TM constraint at 2005.0 (black) and TG constraint (gray). Those corresponding to (a) the first 50 toroidal flow coefficients and (b) the first 50 poloidal flow coefficients are shown here. The coefficient number j is arranged in such a way that $j = 1, 2, 3, 4, 5, \cdots$ corresponds to u_1^0, u_1^{1c}, u_1^{1s}, u_2^0, u_2^{1c}, $\cdots$, where $u_l^{m(c,s)}$ stands for either the toroidal or poloidal flow coefficients with the SH degree l and order m, and (c, s) represents the relevant azimuthal basis function, cosine or sine.

$\boldsymbol{u}_H^{TG}$ grows, however, when these constraints are imposed, particularly to a relatively great extent for the TG constraint. Also plotted in Figure 1 is the RMS $(\| \delta\dot{\boldsymbol{B}} \|_a^2)^{1/2}$ of the SV misfit $\delta\dot{\boldsymbol{B}}$ between the prediction and *GRIMM-2* SV for the whole model period over the spherical surface with the radius of the Earth radius a (in this paper, the overbar denotes the time-average over the whole model period from $t_0 = 2000.0$ to $t_1 = 2010.0$, i.e., $\overline{X} = (t_1 - t_0)^{-1} \int_{t_0}^{t_1} X\, dt$). The TG constraint degrades the fit to SV much more significantly than the TM constraint. Lowering the damping parameter for the TG constraint actually reduces the misfit effectively, but allows $\boldsymbol{u}_H^{NM}$ to enter the flow solution, making the subsequent model inconsistent with the RV equation (3).

[30] We further compare the two constraints by computing the resolution matrix. As we are interested only in the effect of adding the relevant norm Q in resolving the solution, we examine the diagonal elements of the resolution matrix defined by

$$\mathsf{R} = \left(\mathsf{A}_{\dot{\mathsf{b}}}^T \mathsf{C}_{\dot{\mathsf{b}}}^{-1} \mathsf{A}_{\dot{\mathsf{b}}} + \lambda_s \mathsf{D}_s^{-1} + \lambda_t \mathsf{D}_t^{-1} + \lambda_q \mathsf{D}_q^{-1}\right)^{-1} \cdot \left(\mathsf{A}_{\dot{\mathsf{b}}}^T \mathsf{C}_{\dot{\mathsf{b}}}^{-1} \mathsf{A}_{\dot{\mathsf{b}}} + \lambda_s \mathsf{D}_s^{-1} + \lambda_t \mathsf{D}_t^{-1}\right). \quad (21)$$

The diagonal elements of R help in understanding how much of the obtained solution has been controlled by the penalty Q. More specifically, a flow coefficient $(\mathsf{m})_j$ ($j = 1, \cdots, 1566$) is determined fully by the TM constraint or TG constraint, when its corresponding diagonal element in the resolution matrix $(\mathsf{R})_{jj}$ is 0. On the contrary, $(\mathsf{m})_j$ is not at all determined by these constraints, when $(\mathsf{R})_{jj} = 1$. Figures 2a and 2b show (R_{jj}) with regard to the TG constraint and the TM constraint, respectively. They are computed with $\lambda_s = 1.0 \times 10^{-1}$ and $\lambda_q = 1.0 \times 10^{14}$ for both constraints. The choice of λ_q is such that we impose the TG or TM constraint rigorously. As discussed by *Wardinski et al.* [2008], the poloidal flow is predominantly determined by the TG constraint; above all, its zonal components are completely damped. The toroidal flow is basically less affected by the TG constraint, while the degree of the constraint varies more significantly with its mode. The zonal components are entirely free from the TG constraint, but the sectorial components are subject to the constraint to a substantial extent. The TM constraint is distinct from the TG constraint in that the poloidal flow is notably weakly constrained. This can be quantitatively checked through the flow's number of degrees of freedom $\sum_{j=1}^{1566} (\mathsf{R})_{jj}$, which is 729.0 for the TG constraint and 950.0 for the TM constraint (note that these computations equal L_u^2 and $1566 - (L_G(L_G + 2) - L_J(L_J + 2))$, respectively; see Appendix A). Their difference by 221.0 - this equals the number of degrees of freedom for the ageostrophic TM flow $\boldsymbol{u}_H^{ATM}$ - is attributed to the poloidal and toroidal parts by 182.4 and 38.6, respectively. It is thus indicated that the constraint relaxation is largely due to the poloidal flow. The toroidal flow is of course relaxed as well. In fact, all its modes are only marginally controlled by the TM constraint, except for the sectorial components.

[31] We build four flow models, two with the TG constraint, and the other two with the TM constraint. For each constraint, two different SV misfit levels, moderate and tight, are chosen. We name these four models *M-TG-flow*, *T-TG-flow*, *M-TM-flow*, and *T-TM-flow*, for the moderate-fit (*M*) and tight-fit (*T*) models estimated with the TG constraint (*TG*) and TM constraint (*TM*) (see Table 2 for their statistics). The spectra of the *GRIMM-2* SV and the misfit SVs are displayed in Figure 3. We regard all the flow models as consistent with *GRIMM-2*, as they account for the *GRIMM-2* SV acceptably at least up to degree 11. Also plotted in Figure 3 are the spectra of the free decay (used to form $\mathsf{C}_{\dot{\mathsf{b}}}$ in equation (19)) and the non-modeled advection of the truncated small-scale MF. The latter is derived following the protocol of *Eymin and Hulot* [2005]. It is revealed that the non-modeled advection is not as significant as the free decay, which is not the case for the models of *Pais and Jault* [2008]. As the observation and modeling error is predominant in the SV variance at degrees 8–14 in our $\mathsf{C}_{\dot{\mathsf{b}}}$ (section 3, but see also *Holme and Olsen* [2006]), the SV fits at these degrees are much looser than those of Pais et al.'s models. As discussed by them, the large-scale non-modeled

Table 2. The Damping Parameters and Statistics of the Estimated Flow Models[a]

Model	λ_s	λ_q	λ_r	$(\overline{\|\delta\dot{\boldsymbol{B}}\|_a^2})^{1/2}$	$(\overline{\|\boldsymbol{u}_H\|_c^2})^{1/2}$	$\|\boldsymbol{u}_H\|_c$	$\|\boldsymbol{u}_H^{TG}\|_c$	$\|\boldsymbol{u}_H^{AG}\|_c$	$\|\boldsymbol{u}_H^{ATM}\|_c$	$\|\boldsymbol{u}_H^{NM}\|_c$
M-TG-flow	3.0×10^{-2}	1.0×10^{14}	0.0	6.45	12.77	12.88	12.88	0.00	0.00	0.00
M-TM-flow	1.0×10^{-1}	1.0×10^{14}	0.0	3.62	9.40	9.52	9.08	2.85	2.85	0.00
T-TG-flow	5.0×10^{-3}	1.0×10^{14}	0.0	2.13	14.39	14.46	14.46	0.00	0.00	0.00
T-TM-flow	1.0×10^{-2}	1.0×10^{14}	0.0	0.69	10.50	10.54	9.97	3.44	3.44	0.00
Unconstrained-flow	1.0×10^{-1}	0.0	0.0	2.50	9.17	9.24	8.38	3.89	3.09	2.37
Relaxed-TG-flow	1.0×10^{-1}	5.0×10^{1}	0.0	6.48	10.29	10.42	10.34	1.30	1.22	0.45

[a]Here $(\overline{\|\delta\dot{\boldsymbol{B}}\|_a^2})^{1/2}$ and $(\overline{\|\boldsymbol{u}_H\|_c^2})^{1/2}$ are the RMS SV misfit and RMS flow velocity over the model period 2000.0–2010.0, respectively. $\|\boldsymbol{u}_H\|_c$, $\|\boldsymbol{u}_H^{TG}\|_c$, $\|\boldsymbol{u}_H^{AG}\|_c$, $\|\boldsymbol{u}_H^{ATM}\|_c$ and $\|\boldsymbol{u}_H^{NM}\|_c$ are the RMS flow velocities at 2005.0.

advection is attributed primarily to the high flow powers at degrees 15–18, which are required for their tighter SV fit at degrees 11–14. We thus verify a posteriori the dismissal of non-modeled advection in defining $\mathsf{C}_{\dot{b}}$ as equation (19). For the tight-fit modelings, for which the same $\mathsf{C}_{\dot{b}}$ is employed, the non-modeled advection is of course more significant. These flows are nonetheless estimated in a spirit along with [*Holme and Olsen*, 2006; *Olsen and Mandea*, 2008], i.e., attempting to find a model of the core flow that fits a SV model as tightly as possible.

[32] The maps of *M-TG-flow* and *M-TM-flow* at 2005.0 are illustrated in Figure 4. For reference, we also present the maps of two other models: *unconstrained-flow* estimated with the smoothing regularizations alone and *relaxed-TG-flow* estimated by imposing a weak TG constraint (the properties of these models are also given in Table 2). *M-TG-flow* has features that are already well known [e.g., *Holme*, 2007]: azimuthal flows at the equator, strong westward flows in the Atlantic hemisphere, polar vortices, the retrograde vortices below Indian Ocean and North America. *M-TM-flow* includes the dominant westward flow as well, but other typical features of *M-TG-flow* are not evidently visible. The tight-fit models *T-TG-flow* and *T-TM-flow* (whose maps are not shown here) exhibit a little more spatial complexity, but they basically have the same spatial structures as each of their moderate-fit models. The general structure of *M-TM-flow* is similar to that of *unconstrained-flow* or *relaxed-TG-flow*; apparently, *M-TM-flow* involves more azimuthal components near the equator than *unconstrained-flow*, but less than *relaxed-TG-flow*. Interestingly, despite the evident difference in the flow morphologies of *M-TG-flow* and *M-TM-flow*, the latter are composed mostly of the TG part $\boldsymbol{u}_H^{TG}$. Indeed, energy fraction of the ageostrophic part $\boldsymbol{u}_H^{AG}$ of *M-TM-flow* (Figure 5) does not reach 10 percent of the total flow energy (see also Table 2). The ageostrophic TM flow $\boldsymbol{u}_H^{ATM}$, allowed (even slightly) to enter the model space, drastically alters the overall outcome of the inversion, thanks to its effectiveness in enhancing the fit to the SV model.

[33] Figure 6 presents the radial vorticity advections G (equation (4)) associated with the ageostrophic part $\boldsymbol{u}_H^{AG}$ of *M-TM-flow* and *unconstrained-flow* at 2005.0. The computation is done with ρ and Ω given in Table 1. Unlike the *TG-flow* models for which $G = 0$ everywhere, the *TM-flow* models have non-zero G, configured in such a way that they satisfy the RV equation (3) and hence the necessary conditions (5) and (6). We find that amplitudes of G for *M-TM-flow* are comparable to those for *unconstrained-flow* and the rough estimate $|G| \sim 2\rho\Omega\mathcal{V}/\mathcal{L} \sim 10^{-9}$ N/m^4 (Table 1). In contrast, the spatial configuration of G for *M-TM-flow* has

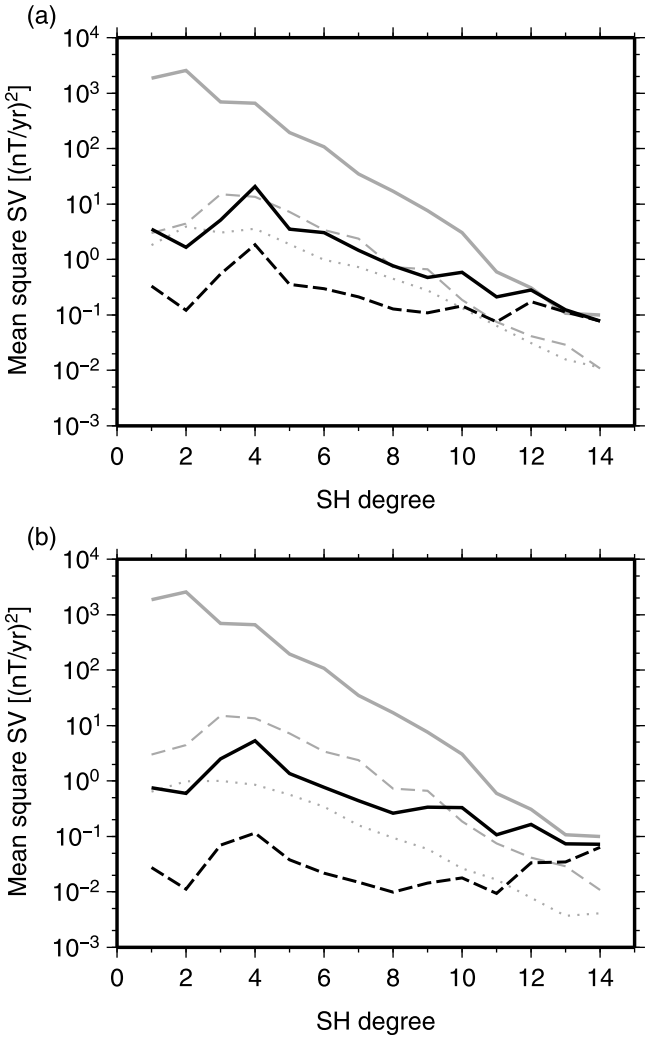

Figure 3. The time-averaged spectra of SV misfit at the Earth's surface $r = a$ calculated from the flow models estimated with (a) the TG constraint and (b) the TM constraint. For each case, the misfit spectra of moderate-fit model (black solid) and tight-fit model (black dashed) are plotted. Also shown are the spectra of the *GRIMM-2* SV (gray solid), and the free decay (gray dashed) and non-modeled advection of the truncated small-scale MF (gray dotted), calculated by following *Holme and Olsen* [2006] and *Eymin and Hulot* [2005], respectively.

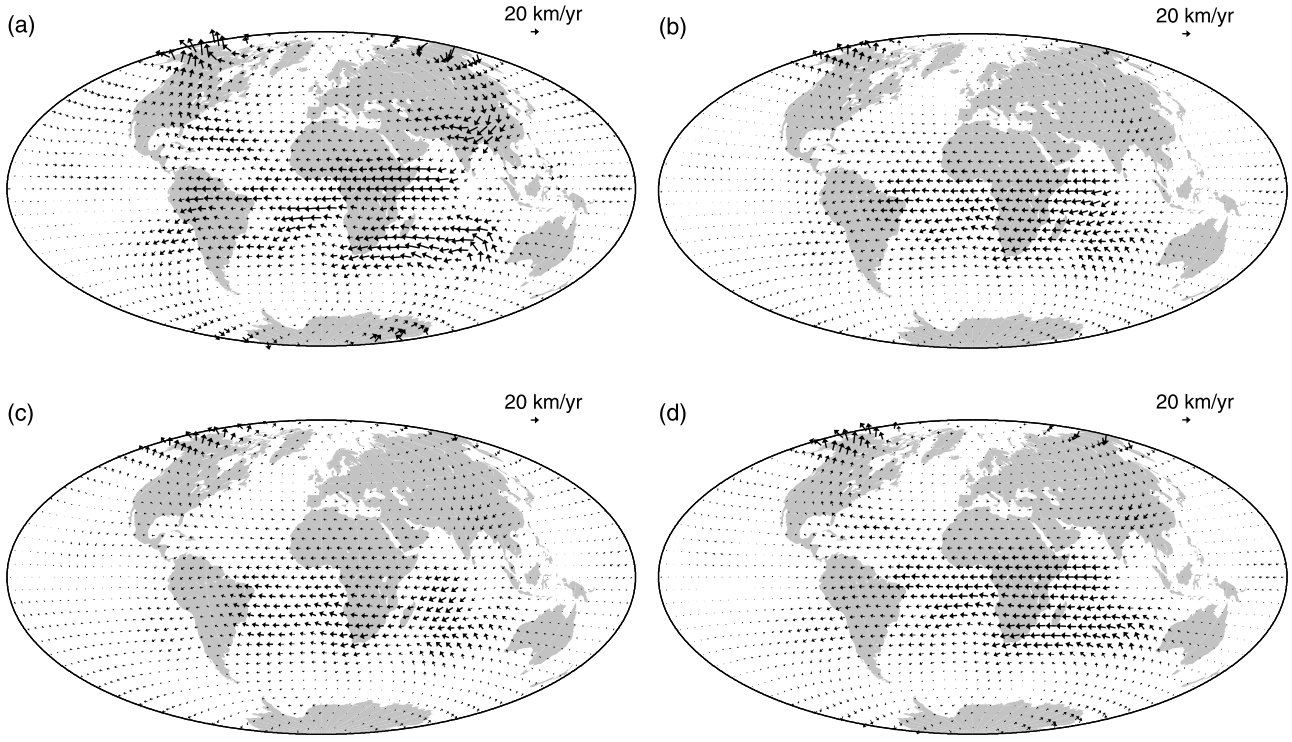

Figure 4. The maps of flow models (a) *M-TG-flow*, (b) *M-TM-flow*, (c) *unconstrained-flow* and (d) *relaxed-TG-flow* at 2005.0.

been properly modified, involving more power in its smaller-scale structures up to degree L_G.

[34] It is worth remarking that the temporal behaviors of *M-TM-flow* and *unconstrained-flow* differs somewhat, despite the similarity of their spatial structures. This may be well illustrated by comparing their zonal toroidal flows, which are the flow components considered to vary most prominently in time [*Jault and Le Mouël*, 1993]. We here present the excess length-of-day (ΔLOD) prediction, computed from these flow components using the formula $\Delta\mathrm{LOD}\ [\mathrm{msec}] = 1.138(t_1^0 + (12/7)t_3^0) + \gamma$, where t_1^0 and t_3^0 (in km/yr) denote the zonal toroidal flow coefficients at degrees 1 and 3, respectively, and γ is an arbitrary constant [*Jackson*, 1997]. The predictions of ΔLOD from *M-TM-flow*, *unconstrained-flow* and *M-TG-flow* are plotted in Figure 7, together with the observed decadal LOD variation. *M-TM-flow* and *M-TG-flow* predict LOD variations in phase with the observation (though their amplitudes does not agree with one another). However, the prediction of the non-constrained flow model fails to have the decreasing trend prior to 2004 seen in the other two predictions and the observed ΔLOD. Their behaviors are consistent with the previous argument that amplitudes of time variations of zonal toroidal flows and their LOD predictions are larger for models built with stronger constraints, as required by fitting the SV more or less equally [*Pais et al.*, 2004].

[35] The LOD predictions of *M-TM-flow* and *M-TG-flow* are well correlated with the time variations of their fully geostrophic flows, i.e., zonal toroidal and equatorially symmetric flows (Figure 8). Further, the variations have a feature of propagating phase from the inner core boundary toward the CMB at the equator, which quite resembles the outward traveling torsional waves observed in numerical simulations [*Wicht and Christensen*, 2010]. These flow variations may be a segment of the fast torsional waves with 6-year periodicity [*Gillet et al.*, 2010]. Comparing the two flow models in Figure 8, we note that *M-TM-flow* exhibits an even more distinct feature of propagation than *M-TG-flow*. The present analysis thus indicates that imposing the TM constraint is certainly useful in estimating a plausible flow model, and is no less reasonable than imposing the TG constraint, at least in reference to the time variations of fully geostrophic flows and predicted ΔLOD.

5. TM Constraint in Combination With Purely Toroidal or Helical Flow Constraint

[36] We have shown in the previous section that the flow model space is allowed to have a significantly greater degree

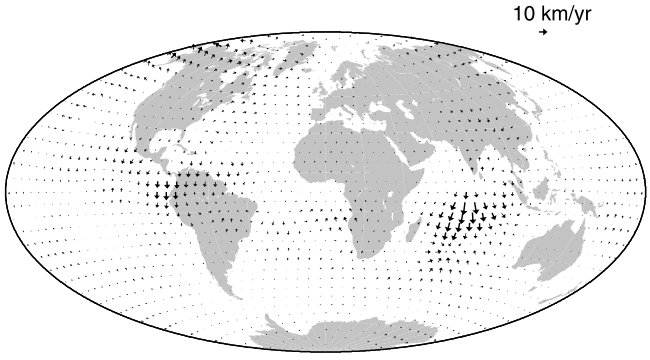

Figure 5. The map of the ageostrophic part of *M-TM-flow* at 2005.0 (Figure 4b). Mind the allow scale different from that in Figure 4.

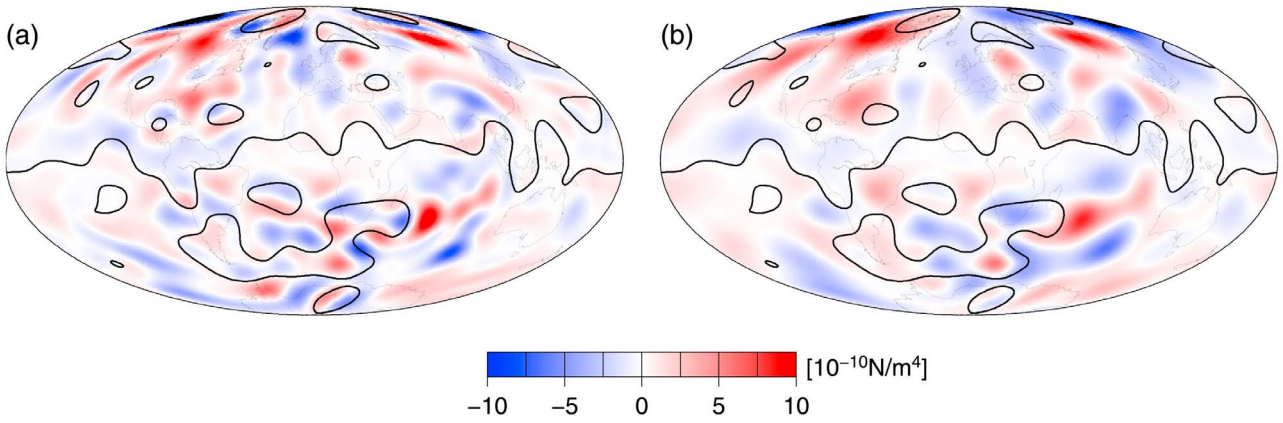

Figure 6. The maps of radial planetary vorticity advection G (in N/m^4) associated with (a) *M-TM-flow* and (b) *unconstrained-flow* at 2005.0. The null-flux curves $B_r = 0$ calculated from the *GRIMM-2* MF model at 2005.0 are illustrated as well.

of freedom by switching the constraint from the TG constraint to the TM constraint, and thereby the norms of SV misfit and model roughness can be further minimized. We are now interested in whether or not this enlarged model space can accommodate further constraints, i.e., the PT or helical constraint which we can add by introducing a nonzero damping parameter λ_r for the norm R in equation (18). We here report flow solutions obtained through a systematic search of reasonable flow models, in which the damping parameters λ_q and λ_r are widely varied. It is found by this analysis that the TM flow model space is still not large enough for the PT constraint to be met simultaneously. The helical flow constraint is also strong, and it is barely compatible with the TM constraint. Some representative flow solutions are listed in Table 3, together with their statistics.

[37] Figure 9a shows the map of model *PT-TM-flow* obtained as a result of the flow inversion with both the TM and PT constraints imposed strictly. Obviously the flow morphology is dominated by the zonal toroidal components, which are irrelevant to the TM constraint. While *PT-TM-flow* captures some flow patterns in common with other flow models, it fails to give an adequate fit to the *GRIMM-2* SV (Table 3), and so is not an acceptable model. When the PT constraint is relaxed, the SV misfit decreases but the solutions still fail to explain the SV as far as the structure with pronounced zonal components as in *PT-TM-flow* remains. A solution compatible with the SV is obtained only when the PT constraint is relaxed to the extent that it is no longer dominated solely by toroidal flow and, intriguingly, that the overall flow configuration resembles that of a model estimated purely with the TG constraint (e.g., *M-TG-flow* as shown in Figure 4a). We conclude that, as far as the *GRIMM-2* MF and SV are concerned, the PT flow assumption is not compatible with the TM constraint.

[38] We see the same difficulty when both the TM and helical constraints are strongly imposed (see Table 3 for the solution *H-TM-flow*, the flow map of which is not presented here). Theoretically, applying a strict helical constraint to the inversion is by itself sufficient for determining the flow uniquely [*Amit and Olson*, 2004]. The TM constraint is not required just for resolving the flow, but it only adds to the SV misfit. Our helical constraint is not strict; the constraint is locally weak near the geographic equator (Appendix B). Even such a weakened helical constraint is not compatible with the TM constraint. Nonetheless, after a systematic exploration for a reasonable model while weakening the helical constraint by reducing the damping parameter λ_r, we spot a range of λ_r for which barely acceptable models come out. One of such models, *relaxed-H-TM-flow* (Figure 9b), satisfies the TM constraint rigorously, and helical constraint to a tolerable degree (Figure 9c). In fact, it is rather reasonable not to seek for a genuine helical flow model. It may not be appropriate to impose a tight agreement in the morphologies of the upwelling ξ and radial *relative* vorticity ζ, because they both tend to be dominated by small-scale ingredients for which the observations should have marginal resolution (the spectra of ξ and ζ vary with SH degree as $\propto l^{-1}$ when the flow spectrum behaves as $\propto l^{-3}$, as forced by the smoothing constraint in this study). Despite the objective

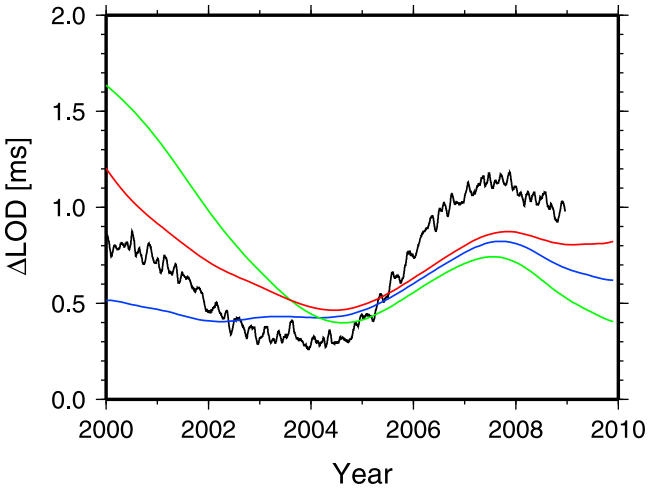

Figure 7. The predicted LOD variations compared with the observed decadal variation of ΔLOD (black) after *Holme and de Viron* [2005], which has been updated up to 2009.0. The predictions are computed from the models *M-TG-flow* (green), *M-TM-flow* (red), and *unconstrained-flow* (blue).

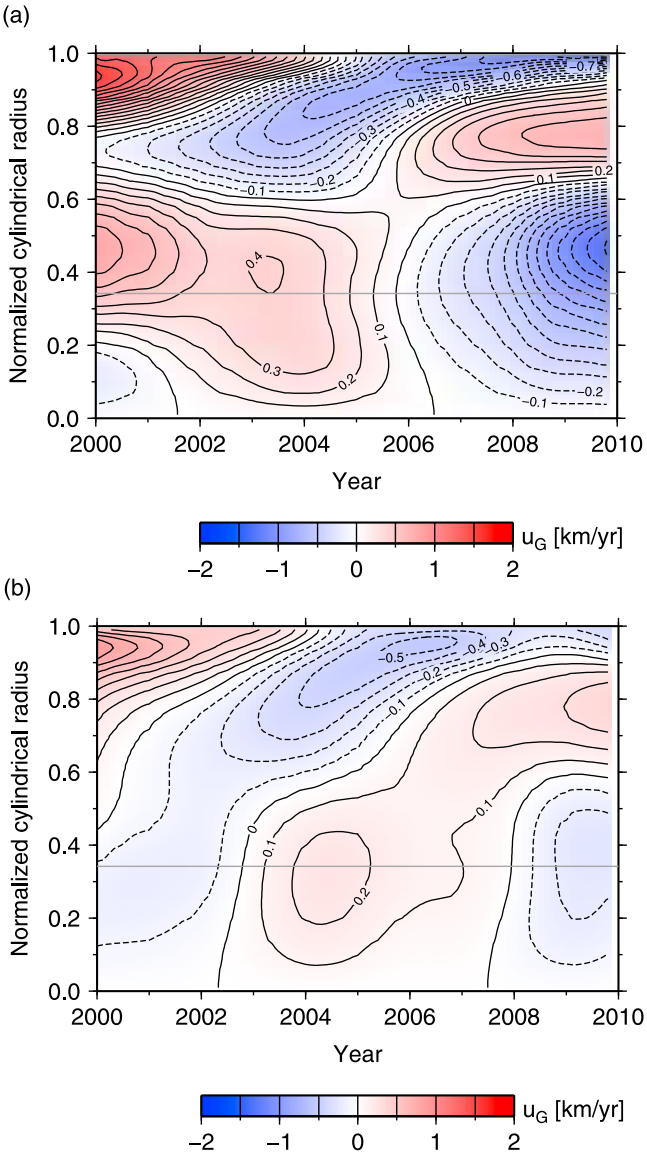

Figure 8. The time-varying part of fully geostrophic flow $\boldsymbol{u}_G$ for the models (a) *M-TG-flow* and (b) *M-TM-flow*, plotted as a function of time and cylindrical radius s normalized by the core radius c (the radius s is defined with respect to the cylindrical coordinate (s, φ, z) with z-axis being the Earth's rotation axis). The gray line indicates the radius of the inner core. The bandpass filter for highlighting 6-year periodicity [*Gillet et al.*, 2010] has not been applied here.

acceptability from the statistics, we still do not favor *relaxed-H-TM-flow*. On top of the relatively poorer fit to the SV, it requires a high degree of spatial complexity, seen as a relatively sharp regional contrast in the velocity distribution of *relaxed-H-TM-flow* (Figure 9b). As far as putting emphasis on simplicity, we have no acceptable helical flow model satisfying the TM constraint as well.

6. Discussion

[39] There are some physical insights drawn from our TM flow modeling. For their discussion we rely on characteristic magnitudes of physical quantities listed in Table 1.

6.1. Implications for the Electric Current and Toroidal Field

[40] A detailed analysis of relaxing the TG constraint has been conducted by *Pais et al.* [2004]. Their approach is basically the same as ours in obtaining *relaxed-TG-flow*. A moderate damping parameter is selected for the TG constraint imposed in the weak-form, so that the solution may have a departure from the TG constraint. Varying the damping parameter systematically, *Pais et al.* [2004] find a broad class of relaxed TG flow solutions consistent with magnetic observations. In order to evaluate the physical viability of these outcomes, they rely on the horizontal components of poloidal electric current density $\boldsymbol{J}_H$ deduced by using the RV equation (3). Their estimated models of $\boldsymbol{J}_H$ (fitting only in the least squares sense to their flow models containing the non-magnetostrophic flow $\boldsymbol{u}_H^{NM}$) provide the RMS intensities $\|\boldsymbol{J}_H\|_c$ over the core surface. They then compute a Joule heating diagnostic of excessive dissipation that contradicts thermodynamic models of the core. Their flow models having only minor deviations from the pure TG are thus preferred, providing an upper bound for the current intensity $\|\boldsymbol{J}_H\|_c \sim 0.4$ A/m^2. This threshold value compares with its simple order-of-magnitude estimate $|\boldsymbol{J}_H| \sim \rho\Omega\mathcal{V}/\mathcal{P} \sim 1$ A/m^2, derived by balancing the Coriolis and Lorentz terms in equation (1) [see also *Benton and Muth*, 1979]. The extreme difficulty of quantifying $\|\boldsymbol{J}_H\|_c$ from magnetic observations may be highlighted by the models of $\boldsymbol{J}_H$ not accepted by *Pais et al.* [2004], for which $\|\boldsymbol{J}_H\|_c$ is greater than the order-of-magnitude estimate $|\boldsymbol{J}_H|$ even by up to 3 order of magnitude. They discuss that such current models are dominated by elements of $\boldsymbol{J}_H$ irrelevant to the RV equation (3).

[41] All through our study we have neither modeled nor analyzed the intensity, morphology or temporal behavior of $\boldsymbol{J}_H$. We have merely sought the flow model space for those compatible with the TM constraint without producing any specific model of $\boldsymbol{J}_H$. Nonetheless, we can at least assess our

Table 3. The Damping Parameters and Statistics of the Flow Models Estimated With the TM Constraint Combined With Additional Constraints[a]

Model	λ_s	λ_q	λ_r	k	$(\overline{\|\delta\dot{\boldsymbol{B}}\|_a^2})^{1/2}$	$(\overline{\|\boldsymbol{u}_H\|_c^2})^{1/2}$
PT-TM-flow	3.0×10^{-2}	1.0×10^{14}	1.0×10^{14}	0.0	21.53	12.51
H-TM-flow	3.0×10^{-2}	1.0×10^{14}	1.0×10^{8}	0.1	43.68	7.84
Relaxed-H-TM-flow	3.0×10^{-2}	1.0×10^{14}	1.0×10^{4}	0.1	12.09	10.83
PT-flow	3.0×10^{-2}	0.0	1.0×10^{14}	0.0	4.35	11.46
H-flow	3.0×10^{-2}	0.0	1.0×10^{8}	0.1	9.75	10.00

[a]Here k is the proportionality factor in the helical flow constraint (B1) (k = 0.0 for the PT constraint). $(\overline{\|\delta\dot{\boldsymbol{B}}\|_a^2})^{1/2}$ and $(\overline{\|\boldsymbol{u}_H\|_c^2})^{1/2}$ are the RMS SV misfit and RMS flow velocity over the model period 2000.0–2010.0, respectively.

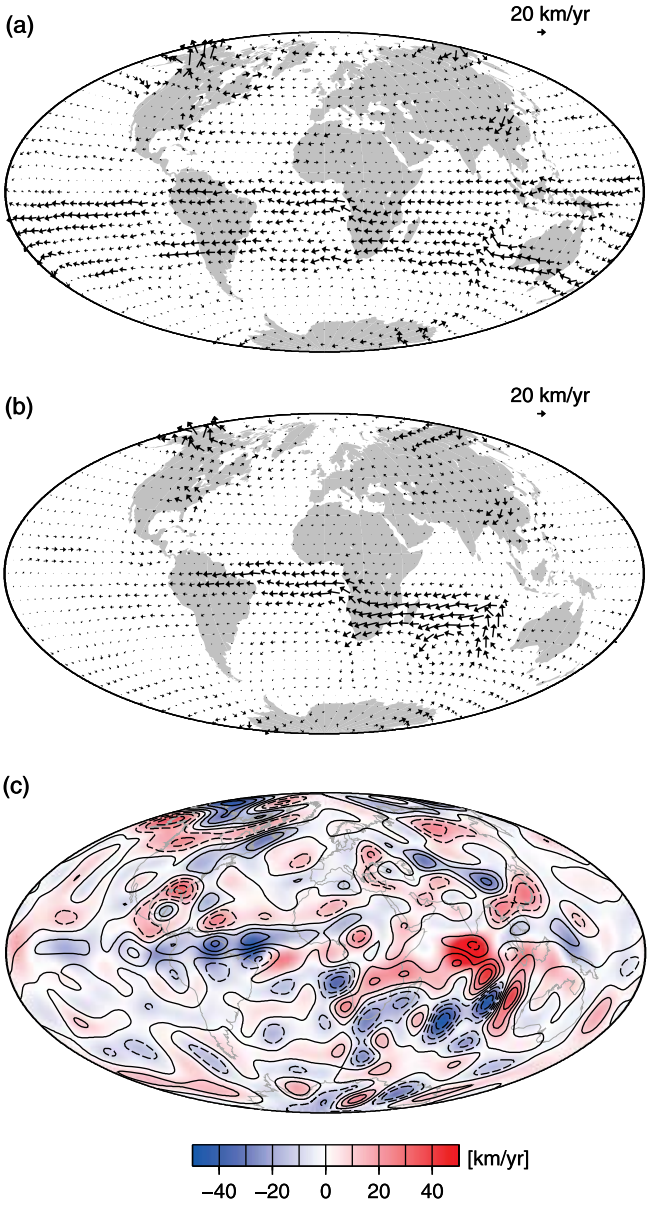

Figure 9. The maps of (a) *PT-TM-flow* and (b) *relaxed-H-TM-flow* at 2005.0, as well as the map of (c) upwelling $c^2\xi$ and relative vorticity $c^2\zeta$ for *relaxed-H-TM-flow* at the same epoch (note the constant factor c^2 for the unit conversion). Here $c^2\xi$ is displayed by the color scale, and $c^2\zeta$ by the contours. The contour interval is 100 km/yr. The solid and dashed contours represent positive and negative values of $c^2\zeta$, respectively.

flow models in reference to the intensity of $\boldsymbol{J}_H$ linked to the ageostrophic TM flow part $\boldsymbol{u}_H^{ATM}$. As the flow models strictly satisfy the TM constraint, we can uniquely derive from them a $\boldsymbol{J}_H$ that fits to $\boldsymbol{u}_H^{ATM}$ perfectly and has minimum energy. The RMS intensities $\|\boldsymbol{J}_H\|_c$ for *M-TM-flow* and *T-TM-flow* at 2005.0 are 0.187 and 0.216A/m^2, respectively. These values are smaller by an order of magnitude than the crude estimate of 1A/m^2 and not in excess of the threshold given by *Pais et al.* [2004]. These models are thus not discounted at least from the thermodynamic context. The toroidal magnetic field $\boldsymbol{B}_T = \nabla \times \mathcal{T}\,\boldsymbol{r}$ then has a radial gradient $\mathcal{T}' \sim \mu(\mathcal{L}/c)\mathcal{J}_P \sim 10^2$ nT/m (the prime represents radial derivative), for the intensity of poloidal current $\mathcal{J}_P \sim 0.2$A/m^2. This is greater by an order of magnitude than the previous estimate ($\mathcal{T}' \sim$ 20nT/m) in favor of the TG assumption, deduced by analyzing the toroidal field expulsion into the mantle [*Gubbins*, 2007] or the electromagnetic core-mantle torque due to toroidal field diffusing into the mantle [*Jault and Le Mouël*, 1991b]. As for our models, the toroidal field reaches ~1 mT at the electromagnetic skin depth δ_c ($\sim\sqrt{\tau/(\mu\sigma_c)} \sim 20$ km) into the core from the CMB. This is essentially inconsistent with the arguments of torsional oscillations with decadal periodicity [*Braginsky*, 1970; *Zatman and Bloxham*, 1997], while it still does not oppose the scenario of *Gillet et al.*'s [2010] fast torsional waves (see section 1).

6.2. Difficulty of PT Flow to Meet the TM Constraint

[42] From the perspective of flow modeling, our study suggests that the fit to SV observation is greatly improved owing to the relaxation of the TG constraint. Particularly, zonal poloidal flow components, which are absent in the purely TG flow model, are allowed to compose a flow model under the TM constraint. These flows effectively advect the axial dipole field which is by far the most powerful, whereas the pure TG flow does not give rise to SV by advecting it. Owing to the high efficiency of SV generation by advecting the axial dipole field, even the toroidal flow components can have somewhat lower complexity under the TM constraint than under the TG constraint, despite the relatively minor degree of freedom additionally given to toroidal flow by switching the constraints.

[43] The significance of the presence of zonal poloidal flow is also relevant to our finding in section 5: PT flow has poorer compatibility with the TM constraint than helical flow. The two additional constraints equally reduce the number of degrees of freedom of the flow by half, yet the complete elimination of poloidal flow due to the PT constraint makes it even harder to accommodate the TM constraint. The difficulty of PT flow to be compatible with the TM constraint may have a lot to do with the fluid dynamics. It is considered that the SV can be attributed to the PT flow, if a stratification layer strong enough to inhibit vertical fluid motion has at least a thickness of electromagnetic skin depth δ_c beneath the CMB [e.g., *Gubbins*, 1991]. In such a layer, the leading order force balance necessarily involves the Lorentz force to form the magnetostrophic state (1), otherwise the toroidal flow would consist of zonal components alone and the magnetic observations could not be explained [*Bloxham*, 1990]. This Lorentz force is very severely regulated by the TM constraint in the absence of zonal poloidal flows such as with PT flow models. Averaging the azimuthal component of equation (1) with respect to a closed path along the longitude at an arbitrary latitude θ_o yields

$$\{-J_\theta B_r\}_{\theta_o} = 2\rho\Omega\cos\theta_o\{u_\theta\}_{\theta_o}, \tag{22}$$

where $\{\cdot\}_{\theta_o}$ represents the mean over the path. As opposed to the helical flow, the PT flow does not include zonal poloidal modes, so $\{u_\theta\}_{\theta_o} = 0$. The mean azimuthal Lorentz force $\{-J_\theta B_r\}_{\theta_o}$ near the core surface must vanish at an arbitrary latitude. Our *PT-TM-flow* is indeed accompanied by $\boldsymbol{J}_H$ in compliance with the very strong condition (22) at the expense of the poor fit to the *GRIMM-2* SV as well as the

dominance of small-scale components for the non-zonal flows. It seems that large-scale non-zonal toroidal flows are relatively unfavorable for the electric current to satisfy equation (22). This is similar to the argument that the PT flow is relatively consistent with the TG constraint at smaller scales [*Gubbins*, 1991]. We argue that the PT assumption is substantially inconsistent with the RV equation (3) in the insulating mantle approximation, despite its high compatibility with magnetic observations [e.g., *Wardinski et al.*, 2008] when the RV equation is not taken into account. It is worth recalling that PT flow is not necessarily ensured by stratification near the core surface; large-scale upwellings can be induced by laterally heterogeneous temperature at the bottom of the mantle [*Gubbins*, 1991; *Jault and Le Mouël*, 1991a]. Even if PT flow is present in a stratified layer extending down to the skin depth δ_c into the core, this would make it hard to explain the observed growth of null-flux patches by the toroidal field expulsion [*Gubbins*, 2007].

[44] There are some factors yet to be discussed that could still provide a compatibility between PT assumption and TM constraint. First of all, we have limited the horizontal electric current $\boldsymbol{J}_H$ to its poloidal components truncated at degree $L_J = 14$. In fact, the number of degrees of freedom for $\boldsymbol{u}_H^{ATM}$ is closely related to that of $\boldsymbol{J}_H$; the former is always smaller by three than the latter, unless the MF has a singular morphology (these are 221 and 224, respectively, in this analysis (Appendix A)). Technically we could include toroidal current, while this would violate the frozen-flux assumption. As there is no controlling the intensity of $\boldsymbol{J}_H$ in our analysis, the parameterized toroidal current could have magnitude comparable with the poloidal current $\mathcal{J}_P \sim 0.2$ A/m^2. This is in considerable excess of its upper bound $\mathcal{J}_T^{\max}$ for the frozen-flux assumption to be verified; the magnetic Reynolds number $R_m = \sigma_c \mathcal{V} \mathcal{P} \mathcal{L}_D / (\mathcal{L} \mathcal{J}_T^{\max})$, where $\mathcal{L}_D$ denotes the length scale relevant to magnetic diffusion, should be of the order of 10^2. Considering horizontal diffusion we have $\mathcal{L}_D \simeq \mathcal{L}$, so $\mathcal{J}_T^{\max} \sim 10^{-3}$ A/m^2, two orders of magnitude smaller than $\mathcal{J}_P$. Radial diffusion, for which δ_c perhaps applies to $\mathcal{L}_D$, indicates even smaller $\mathcal{J}_T^{\max}$, so the toroidal current cannot be among the factors for reconciling the PT assumption with the RV equation.

[45] Another way of releasing the limit of $\boldsymbol{J}_H$ could arise from extending the truncation degree of $\boldsymbol{J}_H$ from 14 up to 28, the highest degree that can interact with B_r truncated at $L_B = 14$ in the RV equation (3). However, this would not make much sense, as it would serve only to grow parameter space and consequently model complexity. As discussed above, magnetic observations carry little information for the intensity, morphology or spectrum of $\boldsymbol{J}_H$. We do not have any other robust prior information about them, either. We here plainly do not expand the analysis beyond the present setting with the poloidal current up to degree 14.

[46] Other possibilities for the consistency of PT flow under the TM constraint might involve reinstating the Lorentz force due to J_r, with $B_r \boldsymbol{J}_H$ in the RV equation (3) now replaced by $B_r \boldsymbol{J}_H - J_r \boldsymbol{B}_H$. This requires discarding the insulating mantle assumption and introducing finite conductivity σ_m of the mantle. The downward continuation of the field is still not seriously affected, because the field in the mantle can be expanded in a parameter $\epsilon \equiv \mu \sigma_m \Delta_m^2 / \tau \sim 0.03$, which represents small first order non-potential field relative to zeroth order potential field [see also *Benton and Whaler*, 1983]. In this case the toroidal field $\boldsymbol{B}_T$ in the core leaks into the mantle, with its amount related to the radial gradient of the toroidal field $\mathcal{T}'$ below the core surface. Within the conductive layer of the mantle (assumed to have a one-dimensional structure $\sigma_m(r)$ with respect to the radius r), $\boldsymbol{B}_T$ satisfies a quasi-static induction equation to the first order (i.e., leading order) in ϵ [*Jault and Le Mouël*, 1991b]. Formally, this equation, together with the boundary conditions (vanishing toroidal field at the upper boundary and continuing horizontal electric field at the bottom boundary), allows us to compute $\boldsymbol{B}_T$ in the layer as well as J_r across the CMB. Here, we make their rough estimates instead. Given the mantle conductance $\Sigma_m \equiv \sigma_m \Delta_m \sim 10^8$ S [e.g., *Gillet et al.*, 2010] (the radial conductivity scale $\Delta_m \sim 100$ km being not larger than the skin depth $\delta_m = \sqrt{\tau / (\mu \sigma_m(c))} \sim 500$ km), we have $|B_T| \sim (\Sigma_m / \sigma_c) \mathcal{T}' \sim 2 \times 10^{-5}$ T and $|J_r| \sim |B_T| / (\mu \mathcal{L}) \sim 2 \times 10^{-5}$ A/m^2, if we adopt $\mathcal{T}' \sim 10^2$ nT/m from our models. As $|B_T| < \mathcal{P}$ and $|J_r| \ll \mathcal{J}_P$, the conducting mantle does not allow $J_r \boldsymbol{B}_H$ at the core surface to have the magnitude comparable to that of $-B_r \boldsymbol{J}_H$. This applies even at the bottom of diffusive layer at depth δ_c, considering the growth rate $\mathcal{T}'$ with depth. Bringing back the neglected Lorentz force does not help defend the PT assumption.

7. Conclusions

[47] We have investigated the effect of relaxing the tangentially geostrophic (TG) constraint into the tangentially magnetostrophic (TM) constraint on the modeling of core surface flow. These constraints are implemented in the flow inversion in the spherical harmonic (SH) domain (spectral method), and the increase in the degree of freedom of the flow due to the change of the constraints is examined. We have drawn three main conclusions from the present study.

[48] First, the flow model space is allowed to have a notably larger degree of freedom under the tangentially magnetostrophic TM constraint than under the TG constraint. The change of the constraints particularly frees the poloidal components of the flow. Accordingly, resulting flow models have significantly simpler morphology under the TM constraint than under the TG constraint for a similar secular variation (SV) misfit. Even with such a simple morphology, models satisfying the TM constraint can be strictly compatible with the radial vorticity (RV) equation (3), with their SV predictions necessarily satisfying the RV constraint (6). We have also shown that our simple flow model *M-TM-flow* estimated under the TM constraint predicts the length-of-day (LOD) variation in good correlation with the observation. It is worth emphasizing that the TM constraint is such that the RV equation should hold at every point in space and time (we have used Gauss-Legendre quadrature to ensure the constraint is met continuously in time). This contrasts with the RV constraint considered so far [*Jackson et al.*, 2007], where the RV equation is reduced to conditions given by invariance of the radial planetary vorticity flux through the null-flux patches over distant epochs.

[49] Second, the intensities of poloidal electric current for our TM flow models required to hold the RV equation do not exceed the upper bound deduced roughly from a thermodynamical analysis. It is nonetheless large enough to let the toroidal magnetic field grow rapidly with depth. The radial gradient of the toroidal field is almost an order of magnitude

greater than previous estimates in favor of the TG assumption. So strong is the field intensity inside the fluid core that decadal modes of the torsional oscillation would no longer be admitted, whereas subdecadal torsional waves are still compatible with our models. In our TM flow modeling, the ageostrophic TM flow, namely the flow connected to the poloidal electric current, has been left entirely free from damping. Alternatively, a TM flow model with diminished poloidal current and toroidal field could be estimated by weakly damping ageostrophic TM flow. Spatial configuration of such a flow model would get closer to that of pure TG flow model.

[50] Third, the number of degrees of freedom allowed to the flow space by the TM constraint is not large enough to adequately accommodate an additional constraint such as purely toroidal (PT) and helical flow constraints. This is a rather important point, as the PT and helical flow assumptions have been commonly used in previous core flow modeling. In particular the PT flow model under the TM constraint is notably dominated by zonal toroidal flows and fails substantially to explain magnetic observations. We attribute the relatively much poorer performance of PT flow in fitting the SV to its lack of poloidal components, to which a considerable degree of freedom would be assigned under the TM constraint. The conclusion is not changed by modifying the RV equations with an inclusion of the toroidal or radial electric current, corresponding to relaxing of the frozen-flux assumption or the electrically insulating mantle assumption, respectively.

[51] In this study, we have solely used *GRIMM-2* to supply B_r in both the RV equation (3) and induction equation (7). This latest field model has been especially designed to image the MF (and its time evolution) at the core surface. However, as is always the case with any other field models based on finite field observations involving noise from other sources, *GRIMM-2* is inevitably noisy and has a limited resolution. Its small-scale field components are damped or truncated. The first of our three conclusions above is presumably robust for any field models adopted. As for the third conclusion, it merits further investigation with respect to different MF models. It is of particular interest, from the point of view of core dynamics as well, whether there can be a core field model compatible with the TM constraint and the PT assumption while retaining a decent fit to observations. Then, one would have to perform a simultaneous modeling of the field, flow and poloidal current under the TM constraint, i.e., an extension of our recent field-flow coestimation under the frozen-flux assumption [*Lesur et al.*, 2010a]. It should bring a firmer answer to the issue of the PT flow assumption, and in addition, a field model allowing for the dynamics near the core surface.

Appendix A: Damping Matrices for the TG and TM Constraints

[52] We derive damping matrices D_{TG}^{-1} and D_{TM}^{-1} for the TG and TM constraints, respectively. For each constraint, these matrices are substituted for D_q^{-1} in the semi-norm Q in the objective function (18). The use of damping matrix for the TG constraint is seen in previous studies [e.g., *Pais et al.*, 2004], in which the radial vorticity advection G (equation (4)) is damped. Instead, we here arrange D_{TG}^{-1} to damp the ageostrophic flow $\boldsymbol{u}_H^{AG}$, a part of the core flow $\boldsymbol{u}_H$ as separated in equation (13); i.e., D_{TG}^{-1} is defined such that $\mathsf{m}^T\mathsf{D}_{TG}^{-1}\mathsf{m} = \|\boldsymbol{u}_H^{AG}\|_c^2$ $(= (4\pi c^2)^{-1} \oint_{r=c} |\boldsymbol{u}_H^{AG}|^2 \, dS)$. Similarly, we derive D_{TM}^{-1} so as to exclusively damp the non-magnetostrophic flow $\boldsymbol{u}_H^{NM}$, a part of $\boldsymbol{u}_H^{AG}$ as separated in equation (14); i.e., D_{TM}^{-1} is defined such that $\mathsf{m}^T\mathsf{D}_{TM}^{-1}\mathsf{m} = \|\boldsymbol{u}_H^{NM}\|_c^2$ $(= (4\pi c^2)^{-1} \oint_{r=c} |\boldsymbol{u}_H^{NM}|^2 \, dS)$.

[53] The flow separations, (13) and (14), are made on the basis of the orthogonality (10) in the spatial domain. The inner product can be written in the SH domain as $\langle \boldsymbol{u}_H^1, \boldsymbol{u}_H^2 \rangle_c = \mathsf{m}_1^T \mathsf{C}_\mathsf{m}^{-1} \mathsf{m}_2$, where $\mathsf{C}_\mathsf{m}^{-1} = \mathrm{diag}[l(l+1)/(2l+1)]$. Similarly, we define the inner products for the quantities G and $\boldsymbol{J}_H$ in terms of their energies; i.e., $\langle G_1, G_2 \rangle_c = \mathsf{g}_1^T \mathsf{C}_\mathsf{g}^{-1} \mathsf{g}_2$ and $\langle \boldsymbol{J}_H^1, \boldsymbol{J}_H^2 \rangle_c = \mathsf{j}_1^T \mathsf{C}_\mathsf{j}^{-1} \mathsf{j}_2$, where $\mathsf{C}_\mathsf{g}^{-1} = \mathrm{diag}[1/(2l+1)]$ and $\mathsf{C}_\mathsf{j}^{-1} = \mathrm{diag}[l(l+1)/(2l+1)]$.

[54] Let us begin with a procedure to derive equation (13) in the SH domain

$$\mathsf{m} = \mathsf{m}_{TG} + \mathsf{m}_{AG} \tag{A1}$$

and the damping matrix D_{TG}^{-1} for the TG constraint. As G and $\boldsymbol{u}_H$ are linearly related (equation (4)), so are they in the SH domain:

$$\mathsf{g} = \mathsf{G}\mathsf{m}\,, \tag{A2}$$

where G is the matrix whose elements are referred to *Pais et al.* [2004]. Note that m cannot be calculated uniquely from g, as the TG part $\boldsymbol{u}_H^{TG}$ of $\boldsymbol{u}_H$ does not contribute to G at all. It is nonetheless possible to obtain the ageostrophic part $\boldsymbol{u}_H^{AG}$ of $\boldsymbol{u}_H$ from a given G, with its uniqueness ensured by selecting the least-norm solution, with regard to minimum $\|\boldsymbol{u}_H^{AG}\|_c^2$ $(= \mathsf{m}_{AG}^T \mathsf{C}_\mathsf{m}^{-1} \mathsf{m}_{AG})$. One can actually calculate the ageostrophic part as

$$\mathsf{m}_{AG} = \mathsf{G}_{AG}^{-1}\mathsf{g}\,. \tag{A3}$$

[55] The generalized inverse matrix G_{AG}^{-1} is derived readily by means of the singular value decomposition (SVD). After a reweighting $\mathsf{G}' = \mathsf{C}_\mathsf{g}^{-1/2} \mathsf{G} \mathsf{C}_\mathsf{m}^{1/2}$, where G' is not of full rank (say, $\mathrm{rank}(\mathsf{G}') = p$), a SVD is performed as

$$\mathsf{G}' = [\mathsf{U}_{AG}|\mathsf{U}_{TG}] \begin{bmatrix} \Lambda_{AG} & 0 \\ 0 & 0 \end{bmatrix} [\mathsf{V}_{AG}|\mathsf{V}_{TG}]^T\,. \tag{A4}$$

[56] The submatrices U_{AG} and V_{AG} consist of p columns, and $[\mathsf{U}_{AG}|\mathsf{U}_{TG}]$ and $[\mathsf{V}_{AG}|\mathsf{V}_{TG}]$ are orthogonal matrices, i.e., $[\mathsf{U}_{AG}|\mathsf{U}_{TG}]^T[\mathsf{U}_{AG}|\mathsf{U}_{TG}] = \mathsf{I}$ and $[\mathsf{V}_{AG}|\mathsf{V}_{TG}]^T[\mathsf{V}_{AG}|\mathsf{V}_{TG}] = \mathsf{I}$. The elements of Λ_{AG} are all zero but the singular values $\lambda_i = (\Lambda_{AG})_{ii} > 0$ for $i = 1, \cdots, p$. The generalized inverse matrix is then given by $\mathsf{G}_{AG}^{-1} = \mathsf{C}_\mathsf{m}^{1/2} \mathsf{V}_{AG} \, \Lambda_{AG}^{-1} \mathsf{U}_{AG}^T \mathsf{C}_\mathsf{g}^{-1/2}$. Further, $\mathsf{m}_{AG} = \mathsf{P}_{AG}\mathsf{m}$ and $\mathsf{m}_{TG} = \mathsf{P}_{TG}\mathsf{m}$, where the projection matrices are given by $\mathsf{P}_{AG} = \mathsf{G}_{AG}^{-1}\mathsf{G} = \mathsf{C}_\mathsf{m}^{1/2} \mathsf{V}_{AG} \mathsf{V}_{AG}^T \mathsf{C}_\mathsf{m}^{-1/2}$ and $\mathsf{P}_{TG} = \mathsf{I} - \mathsf{P}_{AG} = \mathsf{C}_\mathsf{m}^{1/2} \mathsf{V}_{TG} \mathsf{V}_{TG}^T \mathsf{C}_\mathsf{m}^{-1/2}$. As we intend to damp $\|\boldsymbol{u}_H^{AG}\|_c^2$ for the TG constraint, its damping matrix is now derived as $\mathsf{D}_{TG}^{-1} = \mathsf{P}_{AG}^T \mathsf{C}_\mathsf{m}^{-1} \mathsf{P}_{AG}$.

[57] We also make use of SVD to derive equation (14) in the SH domain

$$\mathsf{m}_{AG} = \mathsf{m}_{ATM} + \mathsf{m}_{NM}\,, \tag{A5}$$

and the damping matrix D_{TM}^{-1} for the TM constraint. Combining equations (16) and (A3) yields $\mathsf{m}_{AG} = \mathsf{H}\mathsf{j}$ where $\mathsf{H} = \mathsf{G}_{AG}^{-1}\mathsf{A}_\mathsf{g}$. Note that the electric current j is not uniquely determined from a given m_{AG}, because G is not attributed to such an electric current $\boldsymbol{J}_H^{NM}$ that $B_r\boldsymbol{J}_H^{NM} = \nabla \times V\boldsymbol{r}$, with $V(\theta, \varphi)$ being an arbitrary scalar function. Nonetheless, a SVD allows to find a generalized inverse matrix H_{ATM}^{-1} to specify the relevant part $\mathsf{j}_{ATM} = \mathsf{H}_{ATM}^{-1}\mathsf{m}_{AG}$ with minimum energy. The matrix H is preconditioned as $\mathsf{H}' = \mathsf{V}_{AG}^T\mathsf{C}_\mathsf{m}^{-1/2}\mathsf{H}\mathsf{Z}$. Here the matrix Z defines the model space of electric current $\mathsf{j} = \mathsf{Z}\mathsf{j}^*$, eliminating its elements that cause the Lorentz vorticity forcing $\mathsf{A}_\mathsf{g}\mathsf{J}$ never balanced by the vorticity advection $\mathsf{G}\mathsf{m}_{AG}$. In other words, Z is a matrix that forces j to always satisfy $\mathsf{U}_{TG}^T\mathsf{A}_\mathsf{g}\mathsf{J} = \mathsf{0}$ (we discuss Z further in the last paragraph of Appendix A). The matrix H' may not be of full rank (say, rank(H') = q). Now the SVD is performed as

$$\mathsf{H}' = [\mathsf{U}_{ATM}|\mathsf{U}_{NM}]\begin{bmatrix}\Lambda_{ATM} & 0\\ 0 & 0\end{bmatrix}[\mathsf{V}_{ATM}|\mathsf{V}_{NM}]. \tag{A6}$$

[58] The submatrices U_{ATM} and V_{ATM} consist of q columns, and $[\mathsf{U}_{ATM}|\mathsf{U}_{NM}]$ and $[\mathsf{V}_{ATM}|\mathsf{V}_{NM}]$ are orthogonal matrices, i.e., $[\mathsf{U}_{ATM}|\mathsf{U}_{NM}]^T[\mathsf{U}_{ATM}|\mathsf{U}_{NM}] = \mathsf{I}$ and $[\mathsf{V}_{ATM}|\mathsf{V}_{NM}]^T[\mathsf{V}_{ATM}|\mathsf{V}_{NM}] = \mathsf{I}$. The elements of Λ_{ATM} are all zero but the singular values $\lambda_i = (\Lambda_{ATM})_{ii} > 0$ for $i = 1, \cdots, q$. The generalized inverse matrix is then given by $\mathsf{H}_{ATM}^{-1} = \mathsf{Z}\mathsf{V}_{ATM}\Lambda_{ATM}^{-1}\,\mathsf{U}_{ATM}^T\mathsf{V}_{AG}^T\mathsf{C}_\mathsf{m}^{-1/2}$. Further, $\mathsf{m}_{ATM} = \mathsf{P}_{ATM}\mathsf{m}_{AG}$ and $\mathsf{m}_{NM} = \mathsf{P}_{NM}\mathsf{m}_{AG}$, where the projection matrices are given by $\mathsf{P}_{ATM} = \mathsf{H}\mathsf{H}_{ATM}^{-1} = \mathsf{C}_\mathsf{m}^{1/2}\mathsf{V}_{AG}\mathsf{U}_{ATM}\mathsf{U}_{ATM}^T\mathsf{V}_{AG}^T\mathsf{C}_\mathsf{m}^{-1/2}$ and $\mathsf{P}_{NM} = \mathsf{I} - \mathsf{P}_{ATM} = \mathsf{C}_\mathsf{m}^{1/2}\mathsf{V}_{AG}\mathsf{U}_{NM}\mathsf{U}_{NM}^T\mathsf{V}_{AG}^T\mathsf{C}_\mathsf{m}^{-1/2}$. These matrices have notable properties: $\mathsf{P}_{ATM}\mathsf{P}_{AG} = \mathsf{P}_{AG}\mathsf{P}_{ATM} = \mathsf{P}_{ATM}$, $\mathsf{P}_{NM}\mathsf{P}_{AG} = \mathsf{P}_{AG}\mathsf{P}_{NM} = \mathsf{P}_{NM}$, $\mathsf{P}_{ATM}\mathsf{P}_{TG} = \mathsf{P}_{TG}\mathsf{P}_{ATM} = 0$, and $\mathsf{P}_{NM}\mathsf{P}_{TG} = \mathsf{P}_{TG}\mathsf{P}_{NM} = 0$.

[59] In summary, the classification of an arbitrary flow is implemented as $\mathsf{m} = \mathsf{m}_{TG} + \mathsf{m}_{ATM} + \mathsf{m}_{NM} = \mathsf{P}_{TG}\mathsf{m} + \mathsf{P}_{ATM}\mathsf{m} + \mathsf{P}_{NM}\mathsf{m}$. The flow kinetic energy is accordingly separated as $\mathsf{m}^T\mathsf{C}_\mathsf{m}^{-1}\mathsf{m} = \mathsf{m}_{TG}^T\mathsf{C}_\mathsf{m}^{-1}\mathsf{m}_{TG} + \mathsf{m}_{ATM}^T\mathsf{C}_\mathsf{m}^{-1}\mathsf{m}_{ATM} + \mathsf{m}_{NM}^T\mathsf{C}_\mathsf{m}^{-1}\mathsf{m}_{NM}$. Operating with G on this classification of m, one can correspondingly sort the radial planetary vorticity advection as $\mathsf{g} = \mathsf{g}_{ATM} + \mathsf{g}_{NM} = \mathsf{G}\mathsf{P}_{ATM}\mathsf{m} + \mathsf{G}\mathsf{P}_{NM}\mathsf{m}$ (but note that $\mathsf{g}_{ATM}^T\mathsf{C}_\mathsf{g}^{-1}\mathsf{g}_{NM} \neq 0$). As we intend to damp $\|\boldsymbol{u}_H^{NM}\|_c^2$ (= $\mathsf{m}_{NM}^T\mathsf{C}_\mathsf{m}^{-1}\mathsf{m}_{NM}$) for the TM constraint, its damping matrix proves $\mathsf{D}_{TM}^{-1} = \mathsf{P}_{NM}^T\mathsf{C}_\mathsf{m}^{-1}\mathsf{P}_{NM}$. The selective damping of non-magnetostrophic flow $\boldsymbol{u}_H^{NM}$ is thus realized by introducing the new projection matrix P_{NM}.

[60] In the actual computation, we parameterize the MF and SV Gauss coefficients up to SH degree $L_B = 14$, the toroidal and poloidal flow coefficients up to $L_u = 27$ (i.e., dim[m] = $2L_u(L_u + 2) = 1566$), and the horizontal poloidal electric current $L_J = 14$ (i.e., dim[j] = $L_J(L_J + 2) = 224$). Through equation (A2), the vorticity advection g is generated up to degree $L_G = L_u + 1$, so we should consider the TM constraint up to degree $L_G = 28$ (i.e., dim[g] = $L_G(L_G + 2) = 840$). Based on the above procedure, we derive P_{NM} performing twice the SVD and computing the relevant matrices with their dimensions given below. First, we factorize the 840 × 1566 matrix G' as in equation (A4), to obtain $p = L_u(L_u + 4) = 837$ non-zero singular values. Then we precondition the 1566 × 224 matrix H to obtain the 837 × 221 matrix H', using the 837 × 1566 matrix V_{AG}^T and the 224 × 221 matrix Z. The last matrix reduces the number of degrees of freedom of j by 3 (otherwise j would lead to the Lorentz vorticity forcing $\mathsf{A}_\mathsf{g}\mathsf{J}$ never balanced by the vorticity advection g). In fact, g always has $L_G(L_G + 2) - L_u(L_u + 4) = 3$ components never arising from the flow m: two of them are the sectorial components of G at the highest degree L_G, and the last one consists in its L_G (= 28) zonal components linked with only L_u (= 27) components of the zonal poloidal flow. We then factorize H' as in equation (A6), to find $q = 221$ non-zero singular values for any MF within the modeling period. It eventually turns out that m, m_{TG}, m_{AG}, m_{ATM} and m_{NM} have the degree of freedom dim[m] (= 1566), L_u^2 (= 729), p (= 837), q (= 221) and $p - q$ (= 616), respectively. Therefore, under the TM constraint, the estimated flow model has the number of degrees of freedom 1566 − 616 = 950, which is greater than 729 (i.e., that of the purely TG flow) by 221 (i.e., that of the ageostrophic TM flow).

Appendix B: Damping Matrices for Purely Toroidal and Helical Flows

[61] The helical flow assumption in the core flow inversion is first proposed by *Amit and Olson* [2004], to incorporate the core dynamics implied by the numerical geodynamo experiments. Based on the analytical consideration, they remark that the ratio of the flow upwelling $\xi = \nabla_H \cdot \boldsymbol{u}_H$ to the radial component of *relative* vorticity $\zeta = \hat{\boldsymbol{r}} \cdot \nabla \times \boldsymbol{u}_H$ near the core surface may reflect the helicity typically observed in geodynamo models, particularly outside the tangent cylinder (axial cylinder tangent to the inner core) where there are columnar structures of the fluid vortices [*Olson et al.*, 1999]. They also note that this ratio may be independent of the latitude, except that its sign switches across the geographic equator. The helical flow constraint (HFC) is formulated as

$$\xi = \mp k\,\zeta, \tag{B1}$$

where k is the proportionality factor suggested to be 0.1 to 0.4 and negative and positive signs on the right hand side are valid throughout the northern and southern hemispheres, respectively [*Amit and Olson*, 2004]. The purely toroidal flow constraint is derived from the above constraint when $k = 0$.

[62] For a derivation of the HFC (B1) in the SH domain, it may be useful to introduce a step function with respect to the latitude. Letting $x = \cos\theta$ with θ being the colatitude, we define step functions $\Gamma^{\pm}(x)$ for the range $-1 < x < 1$, such that $\Gamma^+(x) = 0$ and $\Gamma^-(x) = 1$ when $x < x_o$, and $\Gamma^+(x) = 1$ and $\Gamma^-(x) = 0$ when $x > x_o$. These step functions are expanded in Legendre function $P_l(x)$ as $\Gamma^{\pm}(x) = \sum_{l=0}^{\infty}\gamma_l^{\pm}P_l(x)$, where $\gamma_0^{\pm} = (1 \mp x_o)/2$ and $\gamma_l^{\pm} = (P_{l+1}(x_o) \mp P_{l-1}(x_o))/2$ for $l > 0$. For a practical description of the step function, we truncate their series at the Legendre function degree $2L_u = 54$. The ringing due to the truncation is alleviated by replacing $\gamma_l^{\pm}$ with $\tilde{\gamma}_l^{\pm} = \gamma_l^{\pm}/(1 + \varepsilon l^2(l+1)^2)$, where we find 5.0×10^{-6} to be appropriate for ε in the present case. Figure B1 shows the truncated step function $\tilde{\Gamma}^+(x) = \sum_{l=0}^{2L_u}\tilde{\gamma}_l^+P_l(x)$, with the step position $x_o = 0.31$ which corresponds to the latitude 18°N. This function is nearly zero for $x < 0$, so it can be used to mask the southern hemisphere. In Figure B1, we also plot $\tilde{\Gamma}^-(x) = \sum_{l=0}^{2L_u}\tilde{\gamma}_l^-P_l(x)$ with $x_o = -0.31$ (corresponding to 18°S), which is used to mask the northern hemisphere.

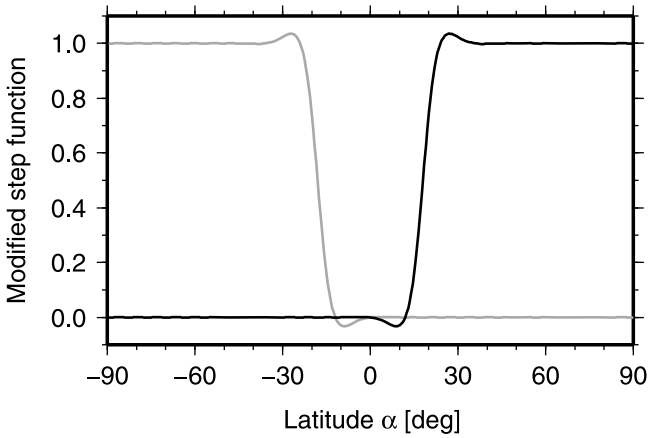

Figure B1. The modified step functions $\tilde{\Gamma}^{+}(x)$ (black) and $\tilde{\Gamma}^{-}(x)$ (gray) truncated at degree 54, as a function of the geographic latitude α in degree ($x = \cos(90° - \alpha)$).

[63] The norm $\mathcal{N}$ to be minimized for the HFC may be strictly written as a sum of surface integrals over the two hemispheres: $\mathcal{N} = (4\pi c^2)^{-1} \int_{\theta<\frac{\pi}{2}} (\xi + k\zeta)^2 \, dS + \int_{\theta>\frac{\pi}{2}} (\xi - k\zeta)^2 \, dS$). Here we approximate it by means of a surface integral over the entire sphere: $\tilde{\mathcal{N}} = (4\pi c^2)^{-1} \oint ((\tilde{\xi}^{+} + k\tilde{\zeta}^{+})^2 + (\tilde{\xi}^{-} - k\tilde{\zeta}^{-})^2) dS$, where $\tilde{\xi}^{\pm} = \tilde{\Gamma}^{\pm}\xi$ and $\tilde{\zeta}^{\pm} = \tilde{\Gamma}^{\pm}\zeta$. As $\xi = -\sum_{l''=1}^{L_u} \sum_{m''=0}^{l''} l''(l''+1) s_{l''}^{m''}$ and $\zeta = -\sum_{l''=1}^{L_u} \sum_{m''=0}^{l''} l''(l''+1) t_{l''}^{m''}$, where $s_{l''}^{m''}$ and $t_{l''}^{m''}$ are poloidal and toroidal flow coefficients, respectively, $\tilde{\xi}^{\pm}$ and $\tilde{\zeta}^{\pm}$ can be expanded in the spherical harmonics Y_l^m up to degree $3L_u = 81$, i.e., $\tilde{\xi}^{\pm} = \sum_{l=0}^{3L_u} \sum_{m=0}^{l} \tilde{\xi}_{l,m}^{\pm} Y_l^m$ and $\tilde{\zeta}^{\pm} = \sum_{l=0}^{3L_u} \sum_{m=0}^{l} \tilde{\zeta}_{l,m}^{\pm} Y_l^m$. The coefficients $\tilde{\xi}_{l,m}^{\pm}$ and $\tilde{\zeta}_{l,m}^{\pm}$ are linear functions of $s_{l''}^{m''}$ and $t_{l''}^{m''}$, respectively:

$$\tilde{\xi}_{l,m}^{\pm} = -\frac{2l+1}{4\pi} \sum_{l'}^{2L_u} \tilde{\gamma}_{l'}^{\pm} \sum_{l''=1}^{L_u} \sum_{m''=0}^{l''} G_{ll'l''}^{m0m''} l''(l''+1) s_{l''}^{m''}$$

$$\tilde{\zeta}_{l,m}^{\pm} = -\frac{2l+1}{4\pi} \sum_{l'}^{2L_u} \tilde{\gamma}_{l'}^{\pm} \sum_{l''=1}^{L_u} \sum_{m''=0}^{l''} G_{ll'l''}^{m0m''} l''(l''+1) t_{l''}^{m''},$$

where $G_{ll'l''}^{mm'm''} = \oint Y_l^m Y_{l'}^{m'} Y_{l''}^{m''} \, dS$ is the Gaunt integral. The approximated HFC norm can then be written in a quadratic form $\tilde{\mathcal{N}} = \mathbf{m}^T \mathbf{D}_r^{-1} \mathbf{m}$ with respect to the flow coefficients $\mathbf{m}$, where $\mathbf{D}_r^{-1}$ is a positive definite matrix (unless $k = 0$) and dependent on the parameter k.

[64] We minimize the objective function (18) with $R(\mathbf{m}) = \lambda_r \tilde{\mathcal{N}}$, where the parameter k is set to be 0 for purely toroidal flow and 0.1 for helical flow. For a PT flow model *PT-flow*, we let the damping parameter $\lambda_r = 10^{14}$, which is large enough to force the solution to be purely toroidal. In contrast, using too a large value for λ_r in the helical flow case leads to a null solution, because of $\mathbf{D}_r^{-1}$ being positive definite, which implies the uniqueness of the HFC in resolving the flow [*Amit and Olson*, 2004]. We select $\lambda_r = 10^8$ for our helical flow model *H-flow*. Other parameters with respect to these flow models are referred to in Table 3.

[65] *PT-flow* has features similar to the models in previous studies (Figure B2a), involving strong westward flows below the regions around Alaska and South Africa [*Holme and Olsen*, 2006; *Wardinski et al.*, 2008]. So we discuss *H-flow* alone, which also has outstanding structures in common with other typical flow models obtained with other constraints (Figure B2b), in particular, with *PT-flow*. The patterns of the upwelling ξ and vorticity ζ match nearly perfectly everywhere outside the equatorial zone (Figure B2c). In the present helical flow modeling, the HFC is not strictly imposed in the vicinity of the equator, as a result of selecting the step positions ±18° for the approximated step functions $\tilde{\Gamma}^{\pm}$ (Figure B1). As mentioned above, these step positions x_o are indeed selected for a technical

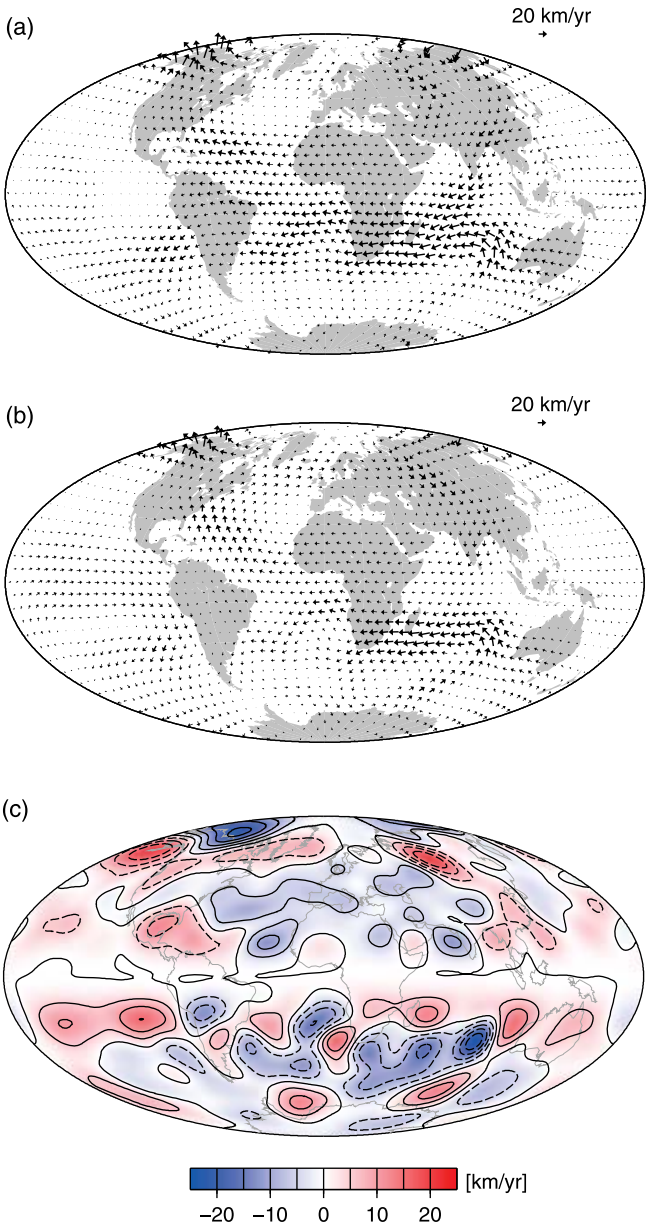

Figure B2. The maps of (a) *PT-flow* and (b) *H-flow* at 2005.0, as well as the map of (c) upwelling $c^2\xi$ and relative vorticity $c^2\zeta$ for *H-flow* at the same epoch (note the constant factor c^2 for a unit conversion). Here $c^2\xi$ is displayed by the color scale, and $c^2\zeta$ by the contours. The contour interval is 50 km/yr. The solid and dashed contours represent positive and negative values of $c^2\zeta$, respectively.

reason arising from the reduced sharpness in the level transition of $\tilde{\Gamma}^{\pm}$; x_o are such that $\tilde{\Gamma}^{\pm}$ stay nearly zero in either of the hemisphere. From a physical perspective, nonetheless, it may also be reasonable to release the HFC around the equator, where the outer boundary nearly parallel to the rotation axis can strongly affect the fluid dynamics, whether the helicity is due to either of the two examples raised by *Amit and Olson* [2004], i.e., the columnar convection or the Ekman suction. The HFC is thus incorporated in the conventional linear core flow inversion method in the SH domain, apart from the original approach in the spatial domain with iterative computations [*Amit and Olson*, 2004]. We can therefore seek for a flow model under the HFC in addition to the TM constraint.

[66] **Acknowledgments.** The authors thank R. Holme and an anonymous reviewer for their insightful comments. Thanks are also due to the Associate Editor, who carefully read the manuscript to improve it. R. Holme kindly provided his data series of the excess length-of-day. V.L. thanks International Space Science Institute for its support of the international team 176. This work is supported by the German Research Foundation (DFG) within the framework of the priority program SPP 1488 "Planetary Magnetism."

References

Amit, H., and P. Olson (2004), Helical core flow from geomagnetic secular variation, *Phys. Earth Planet. Inter.*, *147*, 1–25.

Benton, E. R., and L. A. Muth (1979), On the strength of electric currents and zonal magnetic fields at the top of the Earth's core: Methodology and preliminary estimates, *Phys. Earth Planet. Inter.*, *20*, 127–133.

Benton, E. R., and K. A. Whaler (1983), Rapid diffusion of the poloidal geomagnetic field through the weakly conducting mantle: A perturbation solution, *Geophys. J. R. Astron. Soc.*, *75*, 77–100.

Bloxham, J. (1988), The determination of fluid flow at the core surface from geomagnetic observation, in *Mathematical Geophysics, A Survey of Recent Developments in Seismology and Geodynamics*, edited by V. J. Vlaar et al., pp. 189–208, D. Reidel, Hingham, Mass.

Bloxham, J. (1989), Simple models of fluid flow at the core surface derived from geomagnetic field models, *Geophys. J. Int.*, *99*, 173–182.

Bloxham, J. (1990), On the consequences of strong stable stratification at the top of Earth's outer core, *Geophys. Res. Lett.*, *17*, 2081–2084.

Bloxham, J., and A. Jackson (1991), Fluid flow near the surface of Earth's outer core, *Rev. Geophys.*, *29*, 97–120.

Braginsky, S. I. (1970), Torsional magnetohydrodynamic vibrations in the Earth's core and variations in day length, *Geomagn. Aeron.*, *10*, 3–12.

Busse, F. (1975), A model of the geodynamo, *Geophys. J. R. Astron. Soc.*, *42*, 437–459.

Chambodut, A., C. Eymin, and M. Mandea (2007), Geomagnetic jerks from the Earth's surface to the top of the core, *Earth Planets Space*, *59*, 675–684.

Chulliat, A., and G. Hulot (2000), Local computation of the geostrophic pressure at the top of the core, *Phys. Earth Planet. Inter.*, *117*, 309–328.

Chulliat, A., and G. Hulot (2001), Geomagnetic secular variation generated by a tangentially geostrophic flow under the frozen-flux assumption—I. Necessary conditions, *Geophys. J. Int.*, *147*, 237–246.

Eymin, C., and G. Hulot (2005), On core surface flows inferred from satellite magnetic data, *Phys. Earth Planet. Inter.*, *152*, 200–220.

Gillet, N., M. A. Pais, and D. Jault (2009), Ensemble inversion of time-dependent core flow models, *Geochem. Geophys. Geosyst.*, *10*, Q06004, doi:10.1029/2008GC002290.

Gillet, N., D. Jault, E. Canet, and A. Fournier (2010), Fast torsional waves and strong magnetic field within the Earth's core, *Nature*, *465*, 74–77.

Greff-Lefftz, M., and H. Legros (1995), Core-mante coupling and polar motion, *Phys. Earth Planet. Inter.*, *91*, 273–283.

Gubbins, D. (1991), Dynamics of the secular variation, *Phys. Earth Planet. Inter.*, *68*, 170–182.

Gubbins, D. (2007), Geomagnetic constraint on stratification at the top of the core, *Earth Planets Space*, *59*, 661–664.

Holme, R. (2007), Large scale flow in the core, in *Treatise in Geophysics*, vol. 8, *Core Dynamics*, edited by P. Olson and G. Schubert, pp. 107–129, Elsevier Sci., London.

Holme, R., and O. de Viron (2005), Geomagnetic jerks and a high-resolution length-of-day profile for core studies, *Geophys. J. Int.*, *160*, 435–439.

Holme, R., and N. Olsen (2006), Core surface flow modelling from high-resolution secular variaion, *Geophys. J. Int.*, *166*, 518–528.

Jackson, A. (1996), Kelvin's theorem applied to the Earth's core, *Phil. Trans. R. Soc. A*, *452*, 2195–2201.

Jackson, A. (1997), Time-dependency of tangentially geostrophic core surface motions, *Phys. Earth Planet. Inter.*, *103*, 293–311.

Jackson, A., C. G. Constable, M. R. Walker, and R. L. Parker (2007), Models of Earth's main magnetic field incorprating flux and radial vorticity constraints, *Geophys. J. Int.*, *171*, 133–144.

Jault, D., and J.-L. Le Mouël (1989), The topographic torque associated with a tangentially geostrophic motion at the core surface and inferences on the flow inside the core, *Geophys. Astrophys. Fluid Dyn.*, *48*, 273–296.

Jault, D., and J.-L. Le Mouël (1991a), Physical properties at the top of the Earth's core and core surface motions, *Phys. Earth Planet. Inter.*, *68*, 76–84.

Jault, D., and J.-L. Le Mouël (1991b), Exchange of angular momentum between the core and the mantle, *J. Geomagn. Geoelectr.*, *43*, 111–129.

Jault, D., and J.-L. Le Mouël (1993), Circulation in the liquid core and coupling with the mantle, *Adv. Space Res.*, *13*(11), 221–233.

Le Mouël, J.-L., C. Gire, and T. Madden (1985), Motions at the core surface in geostrophic approximation, *Phys. Earth Planet. Inter.*, *39*, 270–287.

Lesur, V., I. Wardinski, S. Asari, B. Minchev, and M. Mandea (2010a), Modelling the Earth's core magnetic field under flow constraint, *Earth Planets Space*, *62*, 503–516.

Lesur, V., I. Wardinski, M. Hamoudi, and M. Rother (2010b), The second generation of the GFZ Reference Internal Magnetic Model: GRIMM-2, *Earth Planets Space*, *62*, 765–773.

Olsen, N., and M. Mandea (2008), Rapidly changing flows in the Earth's core, *Nat. Geosci.*, *1*, 390–394.

Olson, P., U. Christensen, and G. A. Glatzmaier (1999), Numerical modeling of the geodynamo: Mechanisms of field generation and equilibration, *J. Geophys. Res.*, *104*, 10,383–10,404.

Pais, M. A., and D. Jault (2008), Quasi-geostrophic flows responsible for the secular variaion of the Earth's magnetic field, *Geophys. J. Int.*, *173*, 421–443.

Pais, M. A., O. Oliveira, and F. Nogueira (2004), Nonuniqueness of inverted core-mantle boundary flows and deviations from tangential geosgrophy, *J. Geophys. Res.*, *109*, B08105, doi:10.1029/2004JB003012.

Roberts, P. H., and S. Scott (1965), On the analysis of the secular variation. I. A hydrodynamic constant: Theory, *J. Geomagn. Geoelectr.*, *17*, 137–151.

Wardinski, I., R. Holme, S. Asari, and M. Mandea (2008), The 2003 geomagnetic jerk and its relation to the core surface flows, *Earth Planet Sci. Lett.*, *267*, 468–481.

Whaler, K. A. (1986), Geomagnetic evidence for fluid upwelling at the core-mantle boundary, *Geophys. J. R. Astron. Soc.*, *86*, 563–588.

Wicht, J., and U. R. Christensen (2010), Torsional oscillations in dynamo simulations, *Geophys. J. Int.*, *181*, 1367–1380.

Zatman, S., and J. Bloxham (1997), Torsional oscillations and the magnetic field within the Earth's core, *Nature*, *388*, 760–763.

S. Asari and V. Lesur, Helmholtz-Zentrum Potsdam, Deutsches GeoForschungsZentrum, Telegrafenberg, D-14473 Potsdam, Germany. (asari@gfz-potsdam.de)